MOLECULAR AND CELLULAR BIOLOGY, May 2006, p. 3565–3581 Vol. 26, No. 9
0270-7306/06/$08.00+0 doi:10.1128/MCB.26.9.3565–3581.2006

Essential Dosage-Dependent Functions of the Transcription Factor Yin Yang 1 in Late Embryonic Development and Cell Cycle Progression†

El Bachir Affar,[1]¶ Frédérique Gay,[1]¶ Yujiang Shi,[1]‡ Huifei Liu,[1] Maite Huarte,[1] Su Wu,[1] Tucker Collins,[2] En Li,[3]§ and Yang Shi[1]*

Department of Pathology, Harvard Medical School, Boston, Massachusetts 02115[1]; Department of Pathology, Boston Children's Hospital, Boston, Massachusetts 02115[2]; and Cardiovascular Research Center, Massachusetts General Hospital, and Department of Medicine, Harvard Medical School, Charlestown, Massachusetts 02129[3]

Received 13 October 2005/Returned for modification 28 November 2005/Accepted 11 January 2006

Constitutive ablation of the Yin Yang 1 (YY1) transcription factor in mice results in peri-implantation lethality. In this study, we used homologous recombination to generate knockout mice carrying *yy1* alleles expressing various amounts of YY1. Phenotypic analysis of *yy1* mutant embryos expressing ~75%, ~50%, and ~25% of the normal complement of YY1 identified a dosage-dependent requirement for YY1 during late embryogenesis. Indeed, reduction of YY1 levels impairs embryonic growth and viability in a dose-dependent manner. Analysis of the corresponding mouse embryonic fibroblast cells also revealed a tight correlation between YY1 dosage and cell proliferation, with a complete ablation of YY1 inducing cytokinesis failure and cell cycle arrest. Consistently, RNA interference-mediated inhibition of YY1 in HeLa cells prevents cytokinesis, causes proliferative arrest, and increases cellular sensitivity to various apoptotic agents. Genome-wide expression profiling identified a plethora of YY1 target genes that have been implicated in cell growth, proliferation, cytokinesis, apoptosis, development, and differentiation, suggesting that YY1 coordinates multiple essential biological processes through a complex transcriptional network. These data not only shed new light on the molecular basis for YY1 developmental roles and cellular functions, but also provide insight into the general mechanisms controlling eukaryotic cell proliferation, apoptosis, and differentiation.

Regulation of fundamental cellular processes such as homeostasis, growth, proliferation, apoptosis, and differentiation involves complex networks of transcription factors as well as chromatin-remodeling proteins. Dysregulation of a wide variety of transcriptional regulators has been linked to various developmental defects and diseases, such as tumorigenesis.

Yin Yang 1 (YY1; also called delta, NF-E1, and UCRBP) is a ubiquitously expressed GLI-Krüppel zinc finger-containing transcription factor (23, 28, 44, 60). It is highly conserved from *Xenopus* to humans and has been shown to be the vertebrate homolog of the *Drosophila melanogaster* polycomb group protein Pleiohomeotic (2, 16, 64). YY1 is a multifunctional protein which can act as a transcriptional repressor or activator through combinatorial interactions with various other transcription factors, coactivators, and corepressors as well as chromatin-remodeling complexes displaying opposite functions, including the histone acetyltransferase p300/CBP, the arginine methyltransferase PRMT1, and the histone deacetylases HDAC1 and HDAC2 (4, 9–12, 26, 34, 35, 45, 47, 57, 62, 65, 80, 82, 83).

Since its original isolation, YY1 has been shown to control an ever-growing number of viral and cellular genes, among which are the human immunodeficiency virus type 1 and human papillomavirus oncogenes *E6* and *E7*, several proto-oncogenes (c-*myc*, c-*fos*, and *errb2*), *cdc-6* (cell division cycle 6 homolog), the DNA replication-dependent histone *H3.2* gene, as well as various others (53, 59, 68, 76). With a few exceptions, many YY1 target genes have been characterized based on transient transfection (overexpression experiments and reporter gene assays) and/or in vitro approaches, and most of them have yet to be validated as bona fide YY1 target genes in vivo. Nevertheless, these studies suggest important roles for YY1 in the control of cell growth, proliferation, apoptosis, oncogenic transformation, and differentiation.

Consistent with this hypothesis, YY1 has been shown to functionally interact with c-Myc and E1A oncoproteins (3, 34, 36, 48), as well as to control the stability of the tumor suppressor p53 via a mechanism independent of its transcriptional activity (5, 26, 65). Further supporting the potential involvement of YY1 in tumorigenesis, recent studies suggest that elevated YY1 expression and/or transcriptional activity might contribute to tumor formation and/or progression (11, 14, 21, 56). Altogether, these findings highlight the complex nature of YY1 functions and possible mechanisms of action, but the molecular basis for YY1's biological activities remains largely unknown.

* Corresponding author. Mailing address: Harvard Medical School, Department of Pathology, 77 Avenue Louis Pasteur, Boston, MA 02115. Phone: (617) 432-4318. Fax: (617) 432-6687. E-mail: yang_shi@hms.harvard.edu.

† Supplemental material for this article may be found at http://mcb.asm.org/.

‡ Present address: Department of Biological Chemistry and Molecular Pharmacology, Brigham and Women's Hospital, Boston, MA 02115.

§ Present address: Novartis Institutes for Biomedical Research, Cambridge, MA 02139.

¶ Equal contribution.

Several lines of evidence suggest a critical requirement for YY1 in embryonic development, morphogenesis, and organogenesis. Genetic and biochemical studies have attributed important roles to the *Drosophila* counterpart of YY1, *pleiohomeotic* (*pho*), in embryonic patterning; mutations of *pho* result in homeotic transformations associated with misexpression (i.e., derepression) of homeotic genes (15, 24, 25). YY1 is also essential for neural induction and patterning in *Xenopus laevis* (33, 51). Further emphasizing its critical requirement in embryonic development, we previously reported that constitutive ablation of YY1 in mice results in peri-implantation lethality (20). Heterozygous mice ($yy1^{+/-}$) display a mild developmental delay, and a subset of these animals exhibit neurulation defects and exencephaly (20). While these observations strongly suggest that YY1 might play important additional roles during late embryogenesis, the early embryonic lethality caused by constitutive loss of function precluded investigation of YY1 requirement at later developmental stages.

In this study, we report the generation of conditional knockout mice bearing a $yy1^{flox}$ hypomorphic allele. Genetic crosses with heterozygous mice carrying a wild-type allele and a null allele of YY1 allowed us to generate mutant mice expressing ~75%, ~50%, and ~25% of the normal YY1 level. Phenotypic analysis of these mice and corresponding embryonic fibroblasts revealed a critical, dosage-dependent requirement for YY1 in late embryonic development and cell proliferation. Significantly, complete ablation of YY1 induced cytokinesis failure and cell cycle arrest. Consistent with these findings, genomewide gene expression analysis revealed that YY1 regulates various genes involved in cytokinesis, cell proliferation, and differentiation as well as apoptosis, oncogenic transformation, and DNA repair. Taken together, these data shed new light on YY1 developmental roles, cellular functions, and target genes and set the stage for further investigation of the molecular mechanisms underlying its biological activities.

MATERIALS AND METHODS

Preparation of the targeting construct and generation of *yy1* conditional mice. Isolation of *yy1* genomic clones from the mouse 129/Sv genomic DNA library has been previously described (20). The targeting vector designed to conditionally inactivate the *yy1* locus contained a 5.8-kb SmaI-XmnI fragment for the 5′ arm and a 3.7-kb HindIII-BamHI fragment for the 3′ arm. A 3.4-kb XmnI-HindIII fragment encompassing the proximal promoter region, the entire exon 1 (including both the transcriptional and translational start sites), as well as part of the first intron of the *yy1* locus was inserted between the two homology arms. This 3.4-kb fragment was flanked by two *loxP* sites, allowing Cre-mediated excision of the promoter/exon 1 region of the *yy1* locus. The targeting vector also contained the neomycin resistance gene (Neo) driven by the phosphoglycerate kinase (PGK) promoter and flanked by two Frt sites, allowing Flp-mediated excision of the PGK-Neo cassette.

J1 embryonic stem (ES) cell clones bearing the targeted $yy1^{flox}$ conditional allele and chimeric mice were obtained as previously described (20, 37). Chimeric animals were bred to 129/Sv mice, and heterozygous $yy1^{flox/+}$ offspring were intercrossed to obtain homozygous $yy1^{flox/flox}$ mice. Insertion of a neomycin resistance gene cassette in an intron by gene targeting has previously been reported to alter gene expression by virtue of the potential cryptic splice sites and polyadenylation signals it contains (39). In order to delete the selection cassette, $yy1^{flox/+}$ mice were mated with transgenic "flipper" animals ubiquitously expressing Flp recombinase (22). While homologous recombination events targeting the *yy1* locus were analyzed by Southern blot using external (i.e., derived from a genomic sequence that is not present in the targeting vector) and internal probes (20), Flp- and/or Cre-mediated recombination of the $yy1^{flox}$ and $yy1^{f}$ conditional alleles was monitored using a PCR-based approach. The sequences of the PCR primers and Southern blot probes will be made available upon request.

Histological analysis of hypomorphic mice. Newborn mice were fixed in Bouin solution, dehydrated in ethanol, incubated in xylene, and embedded in paraffin. Lung sections stained with eosin and hematoxylin were observed by light microscopy.

Isolation of MEFs. Mouse embryonic fibroblasts (MEFs) were derived from embryos 13.5 days postcoitum (dpc). Briefly, after removal of the head and internal organs, embryo carcasses were digested in trypsin solution for 30 min at 37°C. After addition of Dulbecco's modified Eagle's medium (DMEM) supplemented with 10% of fetal bovine serum (FBS), the remaining tissues were disrupted by pipetting. The resulting cell suspension was plated and cultured in DMEM supplemented with 10% FBS and antibiotics. Infection with adenovirus-Cre (Gene Transfer Vector Core, University of Iowa) was performed 2 days postisolation. Cells were maintained in the presence of viruses in DMEM containing 5% of FBS for 16 h before being plated for various assays.

RNAi. HeLa cells were transfected with a control or *yy1* RNA interference (RNAi) plasmid (65) using Lipofectamine 2000 (Invitrogen Life Technologies). In some cases (see below), RNAi vectors were mixed with a puromycin resistance-encoding vector, and transfected cells were selected by adding puromycin (1.5 μg/ml; Sigma-Aldrich) to the culture medium for 2 days (65). Cells were then trypsinized and plated for various assays.

Analysis of growth properties. For the colony formation assay, equal numbers (5,000 to 20,000) of MEFs were seeded in six-well plates and cultured for 10 to 12 days. Cell colonies were then stained with a solution containing 30 mg/ml crystal violet, 9 mg/ml ammonium oxalate, and 20% ethanol. The same protocol was used for HeLa cells, but the colony formation assay was performed 14 days after puromycin selection of the transfected cells.

For the MTT [3-(4,5-dimethylthiazolyl-2)-2,5-diphenyltetrazolium bromide; Sigma-Aldrich] assay, equal numbers (10,000 to 30,000) of MEFs were seeded in six-well plates. After 2 to 10 days of culture, cells were incubated in the presence of 400 μg/ml of MTT in DMEM for 30 min at 37°C, allowing metabolic transformation of the MTT by the mitochondria and subsequent formation of an intracellular purple formazan (41). After solubilization of this precipitate in dimethyl sulfoxide, the absorbance was measured at 490 nm.

Analysis of cell viability and apoptotic cell death. Puromycin-selected HeLa cells were treated with various apoptotic agents 4 days after transfection of the RNAi vectors. Briefly, cells were treated with 200 nM of staurosporine (Sigma-Aldrich), 100 μM of etoposide (Sigma-Aldrich), 100 ng/ml of Fas ligand (Alexis Corporation), or 10 μg/ml of tumor necrosis factor alpha (R&D Systems) and harvested at various time points posttreatment. While viable cells were trypsinized and counted, apoptotic cell death was quantified by Western blot analysis of poly(ADP-ribose) polymerase (PARP) cleavage.

Flow cytometry analysis. The DNA content of MEF cells and puromycin-selected HeLa cells was analyzed essentially according to Shah et al. (58). Briefly, cells were harvested by trypsinization 4 days postinfection by adenovirus-Cre or posttransfection of the RNAi vectors and fixed with 50% ethanol. After one wash with phosphate-buffered saline (PBS), cells were treated with RNase A (100 μg/ml; Sigma-Aldrich) for 30 min at 37°C, stained with 50 μg/ml propidium iodide (Sigma-Aldrich), and analyzed with a FACSCalibur machine and Cellquest software (Becton Dickinson).

Bromodeoxyuridine incorporation and indirect immunofluorescence. MEFs and unselected RNAi-treated HeLa cells were cultured on coverslips and incubated with 10 μM bromodeoxyuridine (5-bromo-2′-deoxyuridine; Sigma-Aldrich) for 4 h prior to fixation in a 3% paraformaldehyde solution for 20 min. Cells were then permeabilized with 0.5% of NP-40 in PBS for 20 min and washed with PBS containing 0.1% NP-40. The cells were further treated with 4 M HCl for 30 min, followed by one wash with PBS and another wash with 100 mM borax solution. After an additional wash in PBS containing 0.1% NP-40, cells were incubated in blocking solution (PBS containing 0.1% NP-40 and 10% of FBS) and costained with a mouse monoclonal antibromodeoxyuridine (BU33; Sigma-Aldrich) and a rabbit polyclonal anti-YY1 (H414; Santa Cruz Biotechnology, Inc.).

Expression of various cell cycle markers was analyzed by immunostaining of HeLa cells, using antibodies directed against PCNA (PC10; Santa Cruz Biotechnology, Inc.), cyclin B1 (GNS1; Santa Cruz Biotechnology, Inc.), cyclin E (HE12; Santa Cruz Biotechnology, Inc.), phosphorylated (Ser10) histone H3 (06-570; Upstate Cell Signaling Solutions), α-tubulin (B512; Sigma-Aldrich), or YY1 (H10; Santa Cruz Biotechnology, Inc.). With the exception of cyclin E immunodetection, which required methanol fixation, all immunofluorescence experiments were conducted on paraformaldehyde-fixed HeLa cells, as described previously (66).

Western blot analysis. Total cell extracts were prepared in lysis buffer (50 mM Tris-HCl, pH 7.3; 5 mM EDTA; 50 mM KCl; 0.1% NP-40; 1 mM phenylmethylsulfonyl fluoride; 1 mM dithiothreitol) supplemented with a complete antipro-

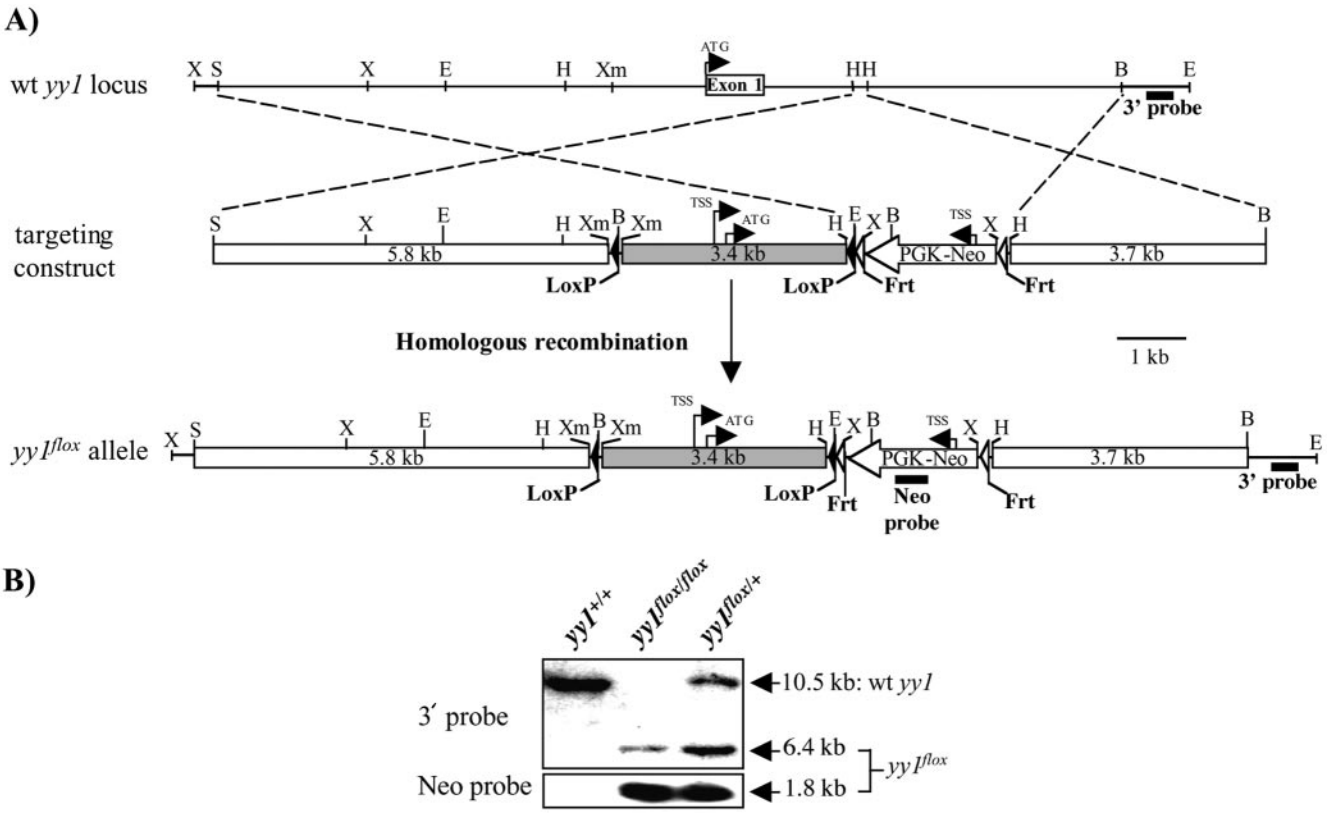

FIG. 1. Conditional targeted disruption of the mouse *yy1* locus. (A) Schematic representation of the mouse *yy1* locus and targeting strategy: genomic organization of a 15-kilobase fragment of the wild-type (wt) *yy1* allele, the targeting vector, and the targeted $yy1^{flox}$ allele obtained after homologous recombination. In addition to the 5.8-kb and 3.7-kb homology arms, the targeting vector contains a 3.4-kb genomic fragment encompassing the promoter-proximal region, the entire exon 1, as well as part of the first intron of the *yy1* locus. The targeting vector also contains two *loxP* sites (black triangles), a neomycin resistance gene (Neo) driven by the PGK promoter, and two Frt sites (white triangles) flanking the Neo cassette. Restriction enzymes sites: B, BamHI; E, EcoRV; S, SmaI; X, XbaI; H, HindIII; Xm, XmnI. The transcription start site (TSS) and translation start site (ATG) are represented by arrows; the 3′ and Neo hybridization probes used for genotyping and the size of a 1-kilobase fragment are also shown. (B) Identification of the $yy1^{flox}$ targeted allele by Southern blot. Genomic DNAs from wild-type ($yy1^{+/+}$) and mutant mice were digested with EcoRV or XbaI and subsequently hybridized with the 3′ probe and Neo probe, respectively. The sizes of the fragments corresponding to the wt and $yy1^{flox}$ alleles are indicated in kilobases.

tease cocktail (Roche Diagnostics), and protein concentration was assessed by Bradford assay. Sodium dodecyl sulfate-polyacrylamide gel electrophoresis, Western blotting, and peroxidase-based chemiluminescence detection were conducted according to standard laboratory procedures. Anti-YY1 (H414 and H10) and anti-PARP (F2) were from Santa Cruz (Santa Cruz Biotechnology, Inc.), the anti-lamin A and C antibody (2032) was from Cell Signaling (Cell Signaling Technology, Inc.), and the antiactin antibody (MAB1501) was from Chemicon International Inc. p53 induction was analyzed using an anti-p53 antibody (PAB240; Santa Cruz Biotechnology, Inc.), adriamycin treatment (2 μg/ml for 10 h) being used as a positive control. Densitometry analysis of YY1 protein levels in tissues and MEFs was performed using a digital camera coupled with band quantification software (Quantity One; Bio-Rad).

Microarray. MEFs were isolated from three wild-type ($yy1^{+/+}$) embryos and compound heterozygous mutant ($yy1^{flox/-}$) littermates, and RNA samples were prepared 4 days postisolation. Briefly, RNAs were prepared using Trizol reagent (Life Technologies) and the RNeasy kit (QIAGEN). cDNAs were generated from total RNAs with the Superscript Choice system (Gibco BRL Life Technologies) and T7-oligo$(dT)_{24}$ primers. Subsequently, biotin-labeled cRNAs were synthesized using a BioArray high-yield RNA transcript labeling kit (Enzo Diagnostic, Inc.). After cleanup, fragmentation, and quality controls, the fragmented cRNAs were subjected to hybridization with a DNA-Chip mouse genome 430A array (Affymetrix) containing over 22,600 probe sets corresponding to transcripts and variants from approximately 15,000 well-characterized mouse genes. Data analysis was performed using DNA-Chip expression analysis software. Briefly, after determining the presence call and average differentiation parameters of each gene, gene expression levels from $yy1^{+/+}$ and $yy1^{flox/-}$ MEFs were subjected to comparative analysis.

RT-PCR analysis. Reverse transcription (RT)-PCR analysis was performed to compare the mRNA expression levels of putative YY1 target genes in $yy1^{+/+}$ and $yy1^{flox/-}$ MEFs 4 days postisolation, as well as in Cre-treated $yy1^{+/+}$ and $yy1^{f/f}$ MEFs 6 days postinfection. Reverse transcription was carried out with 2 μg of total RNA (prepared as described above) using the Superscript III reverse transcriptase and oligo$(dT)_{12–18}$ primers (Invitrogen Life Technologies). Once the semiquantitative conditions were set up, equivalent amounts of $yy1^{+/+}$, $yy1^{f/f}$ and $yy1^{flox/-}$ RT products were submitted to amplification with various sets of PCR primers, and the PCR products were analyzed on ethidium bromide-stained agarose gels. The sequences of the PCR primers will be made available upon request.

RESULTS

Conditional targeted disruption of the *yy1* locus. To circumvent the early embryonic lethality of conventional $yy1^{-/-}$ knockout mice (20) and gain further insights into YY1 biological functions during development, we generated a conditional allele based on the Cre/*loxP* knockout system (52). Deletion of exon 1 of *yy1*, which contains the translation initiation site (Fig. 1A) and encodes more than 50% of the protein, has been

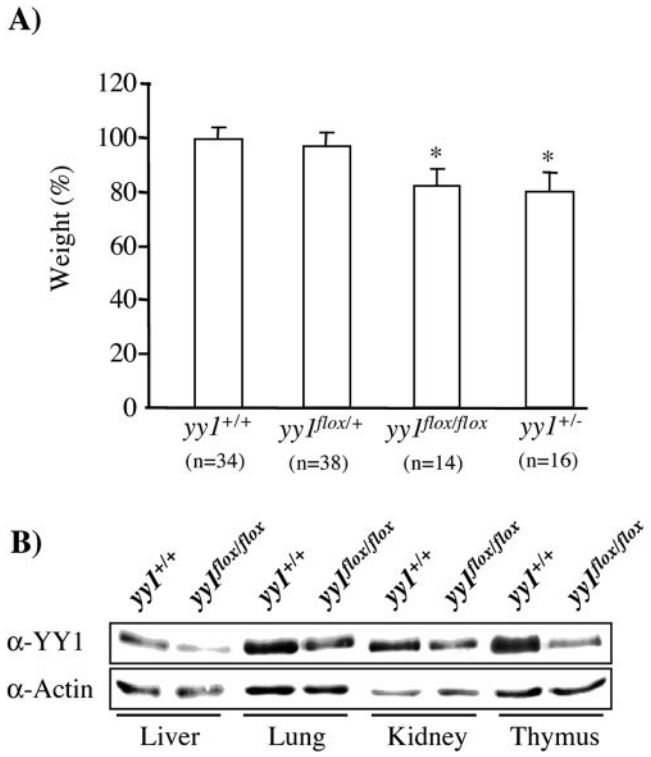

FIG. 2. Hypomorphism of the *yy1*^{flox} allele. (A) Weight of the conditional knockout mice. Heterozygous *yy1*$^{flox/+}$ mice were intercrossed, and the weight of their offspring was determined 3 to 6 weeks after birth. The weight of mice heterozygous for the constitutive *yy1* knockout allele (*yy1*$^{+/-}$) generated from independent crosses is shown as a comparison. Within each litter, the weight of the mutant (*yy1*$^{flox/+}$, *yy1*$^{flox/flox}$, and *yy1*$^{+/-}$) mice was expressed as the percentage of the average weight of their wild-type (*yy1*$^{+/+}$) littermates of the same sex. Each bar corresponds to the mean ± standard deviation of *n* mice, with values obtained from several (>5) independent crosses. *, $P < 0.001$, *yy1*$^{flox/flox}$ and *yy1*$^{+/-}$ versus *yy1*$^{+/+}$ littermates (Student's *t* test). (B) YY1 expression in the *yy1*$^{flox/flox}$ conditional knockout mice. Western blot analysis of YY1 expression level in various organs harvested from 3-week-old homozygous *yy1*$^{flox/flox}$ mice and their wild-type (*yy1*$^{+/+}$) littermates. YY1 was detected with an anti-YY1 (H414) antibody, and an antiactin (MAB1501) antibody was used to verify equal loading of the protein extracts. Densitometry analysis revealed that the YY1 protein level in the liver, lung, kidney, and thymus of the *yy1*$^{flox/flox}$ mice corresponded to 52%, 46%, 54%, and 46%, respectively, of that detected in tissues isolated from their wild-type littermates.

shown to result in a null *yy1* allele (20). Therefore, we constructed a targeting vector (Fig. 1A) containing a 3.4-kb genomic fragment encompassing the promoter-proximal region, the entire exon 1, as well as part of the first intron of the *yy1* locus. This fragment was inserted between two *loxP* sites, designed to direct Cre-mediated excision of the promoter/exon 1 region of the *yy1* locus. The targeting vector also contained the neomycin resistance gene driven by the phosphoglycerate kinase promoter and flanked by two Frt sites, allowing Flp-mediated excision of the PGK-Neo cassette. As shown in Fig. 1B, homologous recombination events generating the "floxed" (i.e., flanked by *loxP* sites) *yy1* allele were monitored by Southern blot analysis of genomic DNA from wild-type (*yy1*$^{+/+}$), heterozygous (*yy1*$^{flox/+}$), and homozygous *yy1*$^{flox/flox}$ mice, using a 3′ external probe and an internal *neo* probe.

Dosage-dependent functions of YY1 during development. Mice heterozygous for the *yy1*^{flox} conditional allele were born at the expected frequency and developed into fertile adults phenotypically indistinguishable from their wild-type littermates. Genotype analysis of the offspring from heterozygous (*yy1*$^{flox/+}$) intercrosses revealed that the number of *yy1*$^{flox/flox}$ newborn pups represented approximately 74% of that expected according to the Mendelian ratio, suggesting that a small subset of homozygous mice died during embryonic development. The remaining *yy1*$^{flox/flox}$ mice were viable and appeared normal despite a significant reduction in body size and weight (Fig. 2A). This developmental delay is reminiscent of the phenotype displayed by mice heterozygous for the constitutive *yy1* knockout allele (20), raising the possibility that the *yy1*^{flox} allele was hypomorphic. Consistent with this hypothesis, Western blot analysis demonstrated that YY1 expression in various tissues of the *yy1*$^{flox/flox}$ mice was reduced to approximately 50% of that expressed by their wild-type littermates (Fig. 2B).

Since the presence of selection markers in the targeted locus is the most common cause of hypomorphism, the neomycin resistance cassette was removed by intercrossing the *yy1*$^{flox/+}$ mice with "flipper" mice ubiquitously expressing Flp site-specific recombinase (22). Flp-mediated recombination targeting the Frt sites (see Fig. S1 in the supplemental material) allowed us to generate homozygous *yy1*$^{f/f}$ mice, which were born at the expected frequency, were indistinguishable in size and weight from their wild-type littermates, and did not display any other detectable defects (data not shown). As anticipated based on the rescue of the growth retardation phenotype observed after deletion of the PGK-Neo cassette, Western blot analysis revealed that wild-type and *yy1*$^{f/f}$ MEFs expressed identical levels of YY1 protein (see Fig. 4C; see also Fig. S1 in the supplemental material). These data demonstrate that removal of the selection cassette restores normal expression of YY1 and strongly suggest that the *yy1*^{flox} allele is a hypomorphic allele.

Intercrossing of the hypomorphic *yy1*$^{flox/flox}$ mice with *yy1*$^{+/-}$ heterozygotes carrying a null *yy1* allele (20) allowed us to generate compound heterozygous mutant embryos (*yy1*$^{flox/-}$) expressing only approximately 25% of the normal amount of *yy1* mRNA (see Fig. 5; see also Fig. S1 in the supplemental material) and protein (see Fig. 4A and B; see also Fig. S1 in the supplemental material). As shown in Table 1, genotype analysis of the progeny obtained from such crosses demonstrated that the majority of the compound heterozygous mutants (*yy1*$^{flox/-}$) developed beyond the time of implantation (4.5 to 6

TABLE 1. Dosage-dependent requirement for YY1 in embryonic development[a]

Time (dpc)	No. of embryos (no. expected)			
	yy1$^{+/+}$ (100% YY1)	*yy1*$^{flox/+}$ (~75% YY1)	*yy1*$^{+/-}$ (50% YY1)	*yy1*$^{flox/-}$ (~25% YY1)
13.5–14.5	14 (13)	26 (21)	13 (13)	16 (21)
16.5–19.5	7 (6)	39 (31)	6 (6)	21 (31)
Postnatal	55 (43)	139 (105)	51 (43)	52 (105)

[a] Heterozygous *yy1*$^{+/-}$ mice were crossed with *yy1*$^{flox/+}$ and *yy1*$^{flox/flox}$ mice, and the offspring were genotyped at various developmental stages. For each genotype, the number of embryos obtained is compared to that expected according to the Mendelian ratio (shown in parentheses).

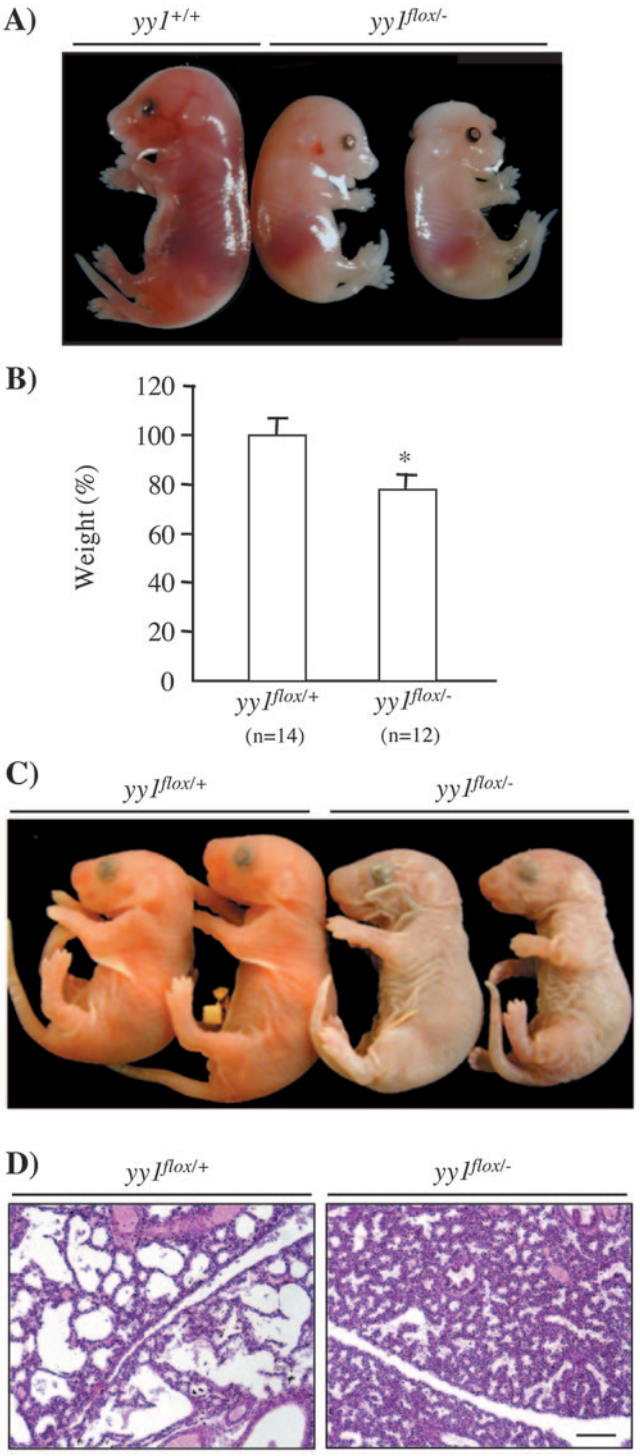

FIG. 3. Phenotype of the hypomorphic $yy1^{flox/-}$ mice. (A) Morphological appearance of the growth-retarded subset of hypomorphic embryos. Heterozygous $yy1^{flox/+}$ mice were crossed with $yy1^{+/-}$ mice, and the morphology of their offspring was observed at 17.5 dpc. While the $yy1^{flox/-}$ embryo shown in the middle is representative of most animals within the growth-retarded subset, the rightmost embryo displays more-severe developmental defects observed in only a few embryos. A wild-type ($yy1^{+/+}$) littermate at the same developmental stage is shown for comparison. (B) Weight of the hypomorphic knockout mice at birth. Homozygous $yy1^{flox/flox}$ mice were crossed with $yy1^{+/-}$ mice, and the weight of their newborn pups was measured. Within each litter, the weight of the $yy1^{flox/-}$ mice was expressed as a percentage of the average weight of their $yy1^{flox/+}$ littermates, whose weights are indistinguishable from those of their wild-type littermates. Each bar corresponds to the mean ± standard deviation of *n* embryos, and values were obtained from several (>5) independent crosses. *, $P < 0.001$, $yy1^{flox/-}$ versus $yy1^{flox/+}$ littermates (Student's *t* test). (C) Gross morphology of the $yy1^{flox/-}$ pups at birth. Homozygous $yy1^{flox/flox}$ mice were crossed with $yy1^{+/-}$ mice, and the morphological appearance of their newborn pups was analyzed. Two $yy1^{flox/+}$ neonates, whose size and appearance are indistinguishable from those of wild-type pups, are shown for comparison. (D). Histological analysis of lungs from $yy1^{flox/-}$ and $yy1^{flox/+}$ newborn littermates stained with hematoxylin and eosin. Bar, 100 μm.

dpc), the stage at which embryonic lethality induced by a complete loss of *yy1* function was previously shown to occur (20). Indeed, comparison of the number of $yy1^{flox/-}$ embryos obtained from our crosses to that predicted by Mendel's law revealed that only ~25% of the $yy1^{flox/-}$ animals died before day 14.5 dpc (Table 1). The discrepancies in the frequency of $yy1^{flox/-}$ embryos expected and obtained became even more pronounced at later stages, indicating that a fraction of embryos died between 13.5 and 14.5 dpc and 16.5 and 19.5 dpc, while another subpopulation died between 16.5 and 19.5 dpc and birth (Table 1). Examination of the morphological appearance of the $yy1^{flox/-}$ mice before birth (17.5 dpc) revealed that a significant subset of $yy1^{flox/-}$ embryos were severely growth retarded and displayed other developmental defects with various degrees of severity (Fig. 3A).

While half of the $yy1^{flox/-}$ animals died during late embryogenesis, the other half survived until birth (Table 1). This subpopulation of $yy1^{flox/-}$ animals displayed only a marginal delay in overall growth, the weight of the newborn $yy1^{flox/-}$ pups representing approximately 80% of that of their wild-type littermates (Fig. 3B). Morphological examination of these embryos did not reveal any obvious developmental defects (Fig. 3C). While the majority of the newborn $yy1^{flox/-}$ animals were alive at birth, they appeared pale and slightly cyanotic compared to their wild-type littermates, suggesting possible abnormalities in hematopoiesis, vascularization, circulation, and/or respiratory function. Importantly, most $yy1^{flox/-}$ animals died within the first day after birth, with the remainder dying within the next 24 h.

To gain further insights into the cause of perinatal lethality of the $yy1^{flox/-}$ mice, embryos were isolated and examined at 19.5 dpc. As expected, most of the wild-type embryos isolated at this stage were able to breathe autonomously. In contrast, the $yy1^{flox/-}$ animals that were alive and reacted to mechanical stimulation at the time of isolation appeared unable to breathe despite frequent gasping and died within an hour postisolation. Postmortem analysis of lungs isolated from newborn $yy1^{flox/-}$ pups indicated that they were not filled with air. Consistently, histological examination revealed collapsed alveoli (Fig. 3D), confirming that the lungs failed to inflate at birth. Together, these results demonstrate an essential, dosage-dependent requirement for YY1 in late embryonic development.

Inhibition of YY1 function impairs cell proliferation in primary cells. As mentioned earlier, generation of the $yy1^{flox}$ hypomorphic allele allowed us to produce mouse strains expressing different levels of YY1. As shown in Fig. 4A and B,

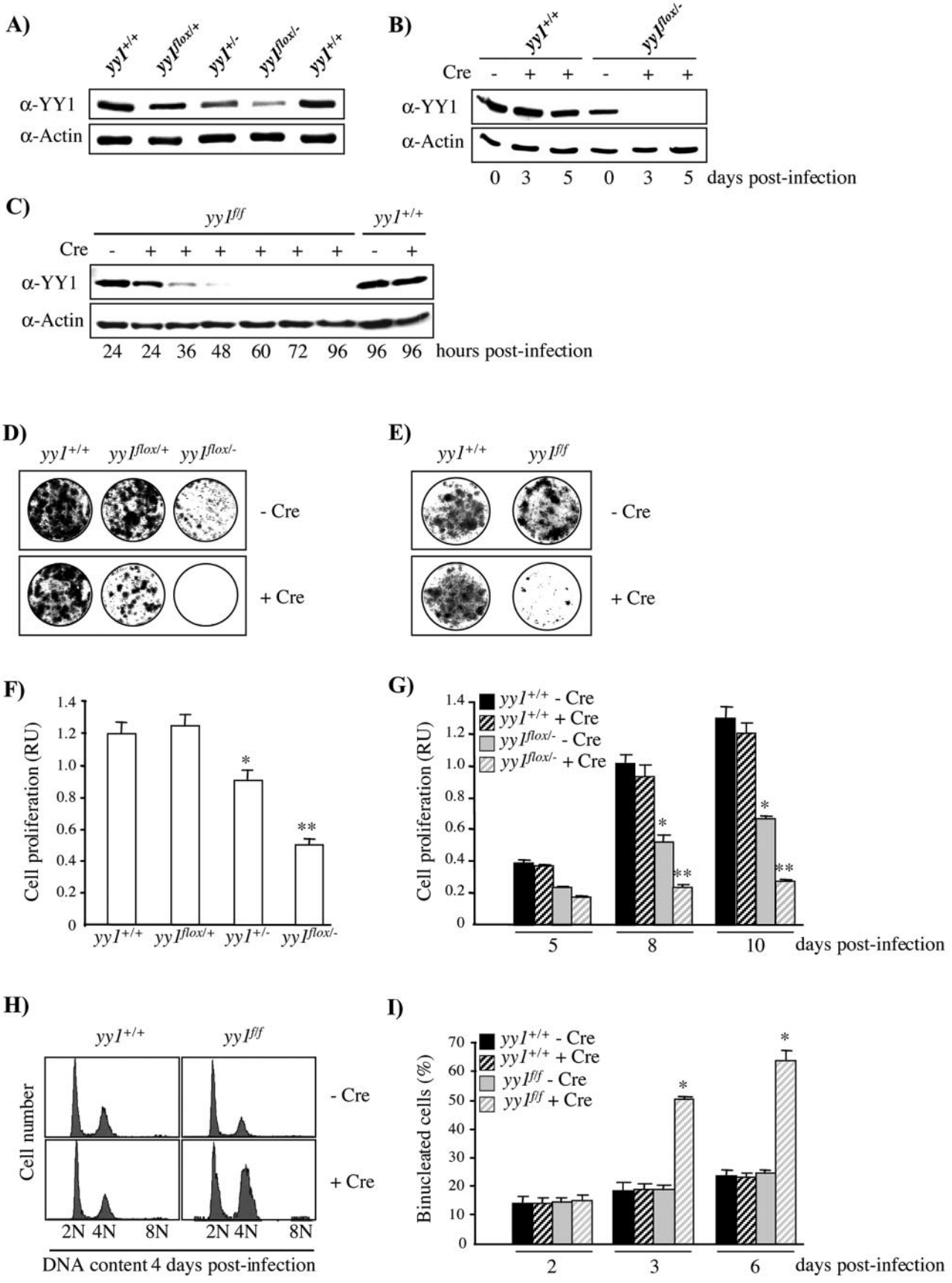
A)
yy1+/+
yy1flox/+
yy1+/-
yy1flox/-
yy1+/+
α-YY1
α-Actin
B)
yy1+/+
yy1flox/-
Cre - + + - + +
α-YY1
α-Actin
0 3 5 0 3 5 days post-infection
C)
yy1f/f
yy1+/+
Cre - + + + + + + - +
α-YY1
α-Actin
24 24 36 48 60 72 96 96 96 hours post-infection
D)
yy1+/+
yy1flox/+
yy1flox/-
- Cre
+ Cre
E)
yy1+/+
yy1f/f
- Cre
+ Cre
F)
Cell proliferation (RU)
1.4
1.2
1.0
0.8
0.6
0.4
0.2
0
*
**
yy1+/+
yy1flox/+
yy1+/-
yy1flox/-
G)
yy1+/+ - Cre
yy1+/+ + Cre
yy1flox/- - Cre
yy1flox/- + Cre
Cell proliferation (RU)
1.4
1.2
1.0
0.8
0.6
0.4
0.2
0
*
**
5
8
10
days post-infection
H)
yy1+/+
yy1f/f
Cell number
- Cre
+ Cre
2N 4N 8N 2N 4N 8N
DNA content 4 days post-infection
I)
yy1+/+ - Cre
yy1+/+ + Cre
yy1f/f - Cre
yy1f/f + Cre
Binucleated cells (%)
70
60
50
40
30
20
10
0
*
*
2
3
6
days post-infection

Western blotting and densitometry analysis of YY1 expression in $yy^{flox/+}$, $yy1^{+/-}$, and $yy1^{flox/-}$ MEFs demonstrated that these cells expressed ~75%, 50%, and ~25% of the normal YY1 level, respectively. In contrast, MEFs isolated from embryos carrying two copies of the conditional $yy1^{f}$ allele (which lacks the PGK-Neo cassette [see above and Fig. S1 in the supplemental material]) expressed YY1 levels indistinguishable from that detected in their wild-type counterparts (Fig. 4C and Fig. S1H in the supplemental material). Time course analysis revealed that infection of $yy1^{flox/-}$ and $yy1^{f/f}$ MEFs with adenovirus-Cre led to a gradual decrease in YY1 protein level, YY1 expression becoming undetectable 2 to 3 days postinfection (Fig. 4B and C; see also Fig. S1 in the supplemental material). To gain insights into YY1 cellular functions, we took advantage of these conditional MEFs and examined the phenotype induced by partial and complete inhibition of YY1.

We first analyzed the viability and growth properties of MEFs of various genotypes in the absence and presence of adenovirus-Cre by a colony-forming assay. As shown in Fig. 4D, untreated $yy1^{flox/+}$ MEFs expressing ~75% of the normal YY1 complement displayed growth properties very similar to those of wild-type cells. While infection of the wild-type cells by adenovirus-Cre did not significantly affect their growth properties, reduction of the YY1 level to ~50% in Cre-treated $yy1^{flox/+}$ MEFs led to a marked decrease in cell proliferation (Fig. 4D). The growth-suppressive effect induced by depletion of YY1 became even more pronounced in untreated $yy1^{flox/-}$ cells expressing ~25% of normal YY1, with complete depletion of YY1 in Cre-treated $yy1^{flox/-}$ MEFs further increasing the severity of this proliferation defect (Fig. 4D). Interestingly, while reduction of YY1 expression to ~25% of the normal complement in untreated $yy1^{flox/-}$ MEFs affected mostly the size of the colonies formed by these cells, a marked decrease in both colony size and colony number was observed after complete depletion of YY1 in $yy1^{flox/-}$ MEFs infected with adenovirus-Cre (Fig. 4D).

Consistent with their ability to express wild-type levels of YY1 (Fig. 4C), no significant differences in cell colony formation were observed when comparing the untreated and $yy1^{f/f}$ MEFs with their wild-type counterparts (Fig. 4E). As expected based on our previous results (Fig. 4D), infection of the $yy1^{f/f}$ MEFs with adenovirus-Cre led to a dramatic decrease in cell colony size and cell colony number (Fig. 4E). Immunofluorescence experiments revealed that the few cell colonies formed by the Cre-treated $yy1^{f/f}$ MEFs were mainly attributable to the presence of YY1-positive cells (i.e., cells that had not been infected by adenovirus-Cre and therefore displayed normal YY1 expression levels and proliferation rates; data not shown). Taken together, these results demonstrate that inhibition of YY1 function in primary cells impairs cell viability and/or proliferation in a dose-dependent manner.

The dosage-dependent effect of YY1 on cell viability and/or proliferation was confirmed by the MTT assay, performed on $yy1^{+/+}$, $yy1^{flox/+}$, $yy1^{+/-}$, and $yy1^{flox/-}$ MEFs expressing 100%, ~75%, 50%, and ~25%, respectively, of the normal amount of YY1 (Fig. 4F). Using a similar approach, we analyzed the growth kinetics of untreated and Cre-treated $yy1^{+/+}$, $yy1^{flox/-}$, and $yy1^{f/f}$ MEFs (Fig. 4G and data not shown). Consistent with our previous observations (Fig. 4D), the MTT assay confirmed that $yy1^{flox/-}$ MEFs expressing ~25% of normal YY1 proliferate at a much lower rate than wild-type cells (Fig. 4G). Despite their impaired growth properties, untreated $yy1^{flox/-}$ MEFs were found to proliferate steadily throughout the course of the experiment (Fig. 4G). In contrast, complete depletion of YY1 in both Cre-treated $yy1^{flox/-}$ MEFs (Fig. 4G) and Cre-treated $yy1^{f/f}$ MEFs (data not shown) abolished cell proliferation.

The decrease in viable cell number caused by depletion of YY1 could result from an increase in cell death, a decrease in cell proliferation, or both. Microscopic observation of the untreated and Cre-treated $yy1^{flox/-}$ and $yy1^{f/f}$ MEFs demonstrated that these cells did not detach and/or die (data not shown). Consistently, these cells did not display any characteristics of apoptotic cells, including nuclear fragmentation or cleavage of lamins A and C, and no significant accumulation of apoptotic (sub-G_0) cells was detected by fluorescence-activated cell sorting (FACS) analysis in either untreated or Cre-treated $yy1^{flox/-}$ and $yy1^{f/f}$ cell populations (Fig. 4H and data not shown).

Besides the appearance of a small subpopulation of cells having an 8N DNA content (see below), the major alteration of cell cycle profile observed upon treatment of the $yy1^{f/f}$ cells with Cre was an accumulation of cells with a 4N DNA content (Fig. 4H). Indeed, 4 days posttreatment, the tetraploid cell population in the $yy1^{f/f}$ MEFs treated with Cre was ~62%, while the percentage of cells with a 4N DNA content in the

FIG. 4. Dose-dependent effect of YY1 on cell proliferation in MEFs. (A to C) Western blot analysis of YY1 expression level in MEFs isolated from $yy1^{flox/+}$, $yy1^{+/-}$, $yy1^{flox/-}$, and $yy1^{f/f}$ littermates and their wild-type ($yy1^{+/+}$) littermates. In panels B and C, MEFs were infected with adenovirus-Cre and harvested at various time points postinfection. In all panels, YY1 was detected with an anti-YY1 antibody (H414), and equal loading of the protein extracts was assessed using an antiactin (MAB1501) antibody. Densitometry analysis revealed that the YY1 protein level in $yy1^{flox/+}$, $yy1^{+/-}$ and $yy1^{flox/-}$ MEFs corresponded to 71%, 54%, and 23%, respectively, of that detected in MEFs isolated from their wild-type littermates. (D and E) Dosage-dependent growth defects of *yy1*-deficient cells. $yy1^{+/+}$, $yy1^{flox/+}$, $yy1^{flox/-}$, and $yy1^{f/f}$ MEFs were infected with adenovirus-Cre, and their growth properties were analyzed by the colony-forming assay. (F) Growth properties of MEFs expressing different levels of YY1. $yy1^{+/+}$, $yy1^{flox/+}$, $yy1^{+/-}$, and $yy1^{flox/-}$ MEFs were subjected to the MTT assay 6 days postisolation. *, $P < 0.014$, $yy1^{+/-}$ versus $yy1^{+/+}$ MEFs; **, $P < 0.001$, $yy1^{flox/-}$ versus $yy1^{+/+}$ and $yy1^{+/-}$ MEFs (Student's *t* test, $n = 6$). (G) Growth kinetics of MEFs after complete depletion of YY1. $yy1^{+/+}$ and $yy1^{flox/-}$ MEFs were infected with adenovirus-Cre, and cell proliferation was assessed by the MTT assay performed at various time points (5, 8, and 10 days) postinfection. In both panels F and G, the results are expressed in relative units (RU) and correspond to the mean ± standard deviation of three values obtained in a representative experiment. *, $P < 0.001$, untreated $yy1^{flox/-}$ versus untreated $yy1^{+/+}$ MEFs; **, $P < 0.001$, Cre-treated $yy1^{flox/-}$ versus Cre-treated $yy1^{+/+}$ and untreated $yy1^{flox/-}$ littermates (Student's *t* test). (H) Cell cycle profile resulting from complete depletion of YY1. MEFs isolated from $yy1^{f/f}$ and $yy1^{+/+}$ littermates were submitted to FACS analysis 4 days postinfection by adenovirus-Cre. (I) Cytokinesis defects induced by complete depletion of YY1. MEFs isolated from $yy1^{+/+}$ and $yy1^{f/f}$ littermates were infected with adenovirus-Cre, and the number of cells with more than one nucleus was counted at 2, 3, and 6 days postinfection. Each value corresponds to the mean ± standard deviation of three values obtained in independent experiments in which at least 500 cells per sample were scored. *, $P < 0.001$, Cre-treated $yy1^{f/f}$ versus Cre-treated $yy1^{+/+}$ MEFs (Student's *t* test).

TABLE 2. Functional classification of YY1 target genes identified in MEF cells expressing 25% of the normal amount of YY1[a]

Gene group and symbol	Gene name and/or description	Accession no.	Fold change
Cell cycle			
Ccna2	Cyclin A2	X75483	−2.66
Ccnb1	Cyclin B1	AU015121	−2.34
Ccnb2	Cyclin B2	AK013312	−2.39
cdca3	Cell division cycle-associated 3	NM_013538	−2.52
Gadd45γ	Growth arrest and DNA-damage-inducible 45 gamma	AK007410	2.76
NP95	Nuclear protein 95	NM_010931	−2.12
p21/Cdkn1a	Cyclin-dependent kinase inhibitor 1A (p21)	NM_007669	3.30
p57/Cdkn1c	Cyclin-dependent kinase inhibitor 1C (p57)	NM_009876	2.02
vav1	*vav1* oncogene	NM_011691	−3.17
cdc25c	Cell division cycle 25 homolog C (*Saccharomyces cerevisiae*)	NM_009860	−2.32
Mitosis and cytokinesis			
Aurka	Aurora kinase A (serine/threonine kinase 6)	U80932	−1.95
Aurkb	Aurora kinase B (serine/threonine kinase 12)	BC003261	−2.47
Survivin/*Birc5*	Survivin/baculoviral IAP repeat-containing 5	BC004702	−2.14
Bub1b	Budding uninhibited by benzimidazoles 1 homolog (*S. cerevisiae*)	AF002823	−2.14
Bub1b/Bubr1	Budding uninhibited by benzimidazoles 1 homolog beta (*S. cerevisiae*)	NM_009773	−2.02
CenpA	Centromere autoantigen A	AV132173	−2.18
CenpH	Centromere autoantigen H	BC025084	−2.60
Cap-g	Chromosome condensation protein G	BB702347	−2.22
Cap-d2	Chromosome condensation-related SMC-associated protein 1	BC025460	−2.19
Incenp	Inner centromere protein	BB418702	−2.08
Kif10/CenpE	Kinesin family member 10/centromere protein E	BG068387	−2.33
Kif11	Kinesin family member 11	BM234447	−2.42
Kif20a	Kinesin family member 20a	NM_009004	−2.09
Kif23	Kinesin family member 23	BG082989	−2.10
Kif2c	Kinesin family member 2C	NM_134471	−2.26
Kif5b	Kinesin family member 5b	BF099632	2.46
Mad2l1	MAD2 (mitotic arrest-deficient homolog)-like 1 (yeast)	NM_019499	−1.85
Nipsnap1	4-Nitrophenylphosphatase domain and nonneuronal SNAP25-like homolog 1	BC010837	−1.73
Plk1	Polo-like kinase 1 homolog (*Drosophila*)	NM_011121	−2.24
Prc1	Protein regulator of cytokinesis 1-like	NM_145150	−1.98
Top2a	Topoisomerase (DNA) II alpha	BM211413	−2.21
Tacc3	Transforming, acidic coiled-coil-containing protein 3	NM_011524	−2.18
DNA replication and repair			
cdc6	Cell division cycle 6 homolog (*S. cerevisiae*)	NM_011799	−3.02
Fen1	Flap structure-specific endonuclease 1	NM_007999	−2.01
Mcmd5/cdc46	Minichromosome maintenance-deficient 5 (*S. cerevisiae*)	NM_008566	−2.76
Mcmd6	Minichromosome maintenance-deficient 6 (*S. cerevisiae*)	NM_008567	−1.85
Mcmd7	Minichromosome maintenance-deficient 7 (*S. cerevisiae*)	NM_008568	−1.88
Mcmd4	Minichromosome maintenance-deficient 4 homolog (*S. cerevisiae*)	NM_008565	−1.94
Mpg	*N*-Methylpurine-DNA glycosylase	BC014754	3.79
Polα1	Polymerase (DNA-directed) alpha 1	NM_008892	−1.89
Polh	Polymerase (DNA-directed) eta (RAD30 related)	NM_030715	−2.09
Polk	Polymerase (DNA-directed) kappa	BC008105	2.15
Rad18	RAD18 homolog (*S. cerevisiae*)	BC011120	−2.03
Rad51ap1	RAD51-associated protein 1	NM_009013	−1.72
Ung	Uracil-DNA glycosylase	NM_011677	−1.86
Apoptosis			
Api5	Apoptosis inhibitor 5	NM_007466	−1.78
Bak1/N-Bak1	Bcl2-antagonist/killer 1 (Bak1)	AF402617	2.55
Biklk	Bcl2-interacting killer-like	BB251824	1.82
Bcl-xL	Bcl2-like 1	U51278	1.81
Casp7	Caspase-7	NM_007611	6.91
Btg2/TIS21	B-cell translocation gene 2, antiproliferative	BG965405	2.59
Clu	Clusterin	AV152288	2.21
Fas/Tnfrsf6	Tumor necrosis factor receptor superfamily, member 6	NM_007987	2.41
Gadd45γ	Growth arrest and DNA-damage inducible 45 gamma	AK007410	2.76
Noxa/Pmaip1	Phorbol-12-myristate-13-acetate-induced protein 1	NM_021451	2.47
Perp	p53 apoptosis effector related to Pmp22	NM_022032	7.61
Pawr/Par4	PRKC, apoptosis, WT1, regulator	BB398886	1.89
Plagl1/Zac1	Pleiomorphic adenoma gene-like 1	NM_009538	1.84
SIP27	Stress-induced protein 27	NM_021897	2.55
Survivin/*Birc5*	Survivin/baculoviral IAP repeat-containing 5	BC004702	−2.14
Tnfrsf10b	Tumor necrosis factor receptor superfamily, member 10b	NM_020275	2.15
Tgm2	Transglutaminase 2, C polypeptide	BB041811	3.01
Cell growth and proliferation			
Btg2/TIS21	B-cell translocation gene 2, antiproliferative	BG965405	2.59
Fos	FBJ osteosarcoma oncogene	NM_010234	3.02
Gfer	Growth factor, erv1 (*S. cerevisiae*)-like (augmenter of liver regeneration)	NM_023040	2.48
Gpc3	Glypican 3	AW107802	2.65
Igfbp5	Insulin-like growth factor binding protein 5	BF225802	−2.87
MKi67	Antigen identified by monoclonal antibody Ki67	X82786	−2.09
Mxd3/Mad3	Max dimerization protein 3	NM_016662	−2.31
Pdgfa	Platelet-derived growth factor alpha	BB371842	2.32
Rbbp4	Retinoblastoma binding protein 4	AU040918	−1.83
RhoE/ArhEe	Ras homolog gene family, member E	NM_028810	2.20

Continued on following page

TABLE 2—*Continued*

Gene group and symbol	Gene name and/or description	Accession no.	Fold change
Src	Rous sarcoma oncogene	NM_001025	1.81
Tgfbi	Transforming growth factor beta induced, 68 kDa	NM_009369	−1.78
Development			
Actc1	Actin, alpha, cardiac	NM_009608	2.37
Alcam	Activated leukocyte cell adhesion molecule	U95030	2.65
BM88	BM88 antigen	NM_021316	3.12
Bmp4	Bone morphogenetic protein 4	NM_007554	2.09
Bmp6	Bone morphogenetic protein 6	NM_007556	1.84
Bdnf	Brain-derived neurotrophic factor	NM_007540	2.69
Ankrd1/Crap	Cardiac responsive adriamycin protein/ankyrin repeat domain 1	NM_013468	2.16
Col9a3	Procollagen, type IX, alpha 3	NM_009936	2.05
Col10a1	Procollagen, type X, alpha 1	NM_009925	1.94
Col19a1	Procollagen, type XIX, alpha 1	NM_007733	3.28
Col15a1	Procollagen, type XV	AF011450	−2.41
Ctnnd2	Catenin delta 2	NM_008729	2.39
Crabp1	Cellular retinoic acid binding protein I	NM_013496	−2.69
CryaB	Crystallin, alpha B	AV016515	2.10
Dkk2	Dickkopf homolog 2 (*Xenopus laevis*)	NM_020265	−2.39
Dlx3	Distal-less homeobox 3	NM_010055	−2.02
Dm15	Dystrophia myotonica kinase, B15	AW108486	2.18
Ebf2	Early B-cell factor 2	U71189	2.29
Efna3	Ephrin A3	AA388313	2.92
Foxm1	Forkhead box M1	NM_008021	−2.28
Hells/Lsh	Helicase, lymphoid specific	NM_008234	−1.99
Hmgb3	High-mobility-group box 3	NM_008253	−3.31
Id4	Inhibitor of DNA binding 4	NM_031166	2.59
Kdr	Kinase insert domain protein receptor	NM_010612	2.74
Lmnb1	Lamin B1	BG064054	−1.97
Lrp2	Low-density lipoprotein receptor-related protein 2	BM119915	2.57
Mmp13	Matrix metalloproteinase 13	NM_008607	−2.11
Mmp2	Matrix metalloproteinase 2	BF147716	2.10
Myd116	Myeloid differentiation primary response gene 116	NM_008654	1.86
Myom1	Myomesin 1	NM_010867	2.36
Myh11	Myosin heavy chain 11, smooth muscle	NM_013607	2.13
Myh6	Myosin heavy chain, cardiac muscle, adult	NM_010856	2.85
Myl1	Myosin light chain, alkali	AK003182	2.34
Mylpf	Myosin light chain, phosphorylatable	NM_016754	2.78
Myh1	Myosin, heavy polypeptide 1	AJ002522	2.21
Myh2	Myosin, heavy polypeptide 2, skeletal muscle, adult	NM_144961	2.25
Myh3	Myosin, heavy polypeptide 3	M74753	4.89
Ngfr	Nerve growth factor receptor	NM_033217	4.24
Nrln1	Neuralin 1	NM_031258	−2.71
Neurod6	Neurogenic differentiation 6	NM_009717	3.98
Nnat	Neuronatin	NM_010923	2.05
Ntf3	Neurotrophin 3	NM_008742	2.71
Pdgfra	Platelet-derived growth factor receptor, alpha polypeptide	AW537708	−2.23
Prox1	Prospero-related homeobox 1	NM_008937	2.36
Rest	RE1-silencing transcription factor	AK004945	−12.47
Sfxn1	Sideroflexin 1	BB478992	−1.98
Sim1	Single-minded 1	NM_011376	2.19
Suv39h2	Suppressor of variegation 3-9 homolog 2 (*Drosophila*)	NM_022724	−4.24
Tslp	Thymic stromal lymphopoietin	NM_021367	2.79
Tgfb2	Transforming growth factor beta 2	NM_009367	1.78
Tgfbr1	Transforming growth factor beta receptor 1	NM_009370	−2.10
Tpm1	Tropomyosin 1, alpha	NM_024427	1.78
Tnnc1	Troponin C, cardiac/slow skeletal	NM_009393	2.04
Tnnc2	Troponin C, fast skeletal	NM_009394	1.70
Tnni1	Troponin 1, skeletal, slow 1	NM_021467	1.86
Tph1	Tryptophan hydroxylase 1	NM_009414	2.50
Wt1	Wilms' tumor homolog	NM_144783	3.25

[a] The putative YY1 target genes identified by comparing gene expression profiles in $yy1^{flox/-}$ and $yy1^{+/+}$ MEFs are organized according to their biological function(s). Only the functional groups most relevant to the phenotypes induced by depletion of YY1 are presented; the complete list of putative target genes is provided in the supplemental material in Table 1. Genes used for validation of the microarray data by RT-PCR are in bold. Genes whose expression was reduced in $yy1^{flox/-}$ MEFs compared to $yy1^{+/+}$ MEFs (i.e., genes activated by YY1) are listed with negative values for changes. Conversely, genes whose expression was induced after partial depletion of YY1 (i.e., genes repressed by YY1) display positive changes.

wild-type (treated or untreated) and untreated $yy1^{f/f}$ MEFs ranged from 26 to 39% (Fig. 4H). Based on these observations, we conclude that inhibition of YY1 function in primary cells does not trigger apoptosis but impairs cellular proliferation in a dosage-dependent manner. Strikingly, complete depletion of YY1 leads to cell cycle arrest and accumulation of tetraploid cells.

YY1 is required for cytokinesis in primary cells. The accumulation of tetraploid cells observed after inhibition of YY1 function could be due to the inability of the cells to progress from G_2 phase to mitosis (blockage at the G_2/M transition), to successfully complete mitosis (mitotic arrest, failure of chromosome segregation), to initiate or complete cytokinesis, or to enter G_1 phase. To characterize the proliferative arrest caused by depletion of YY1 in more detail, we examined the cellular and nuclear morphology of the YY1-depleted cells by phase-contrast light microscopy and fluorescence microscopy after 4′,6′-diamidino-2-phenylindole (DAPI) staining. Most cells

had nuclei with uncondensed chromosomes, arguing against mitotic arrest (data not shown). However, depletion of YY1 resulted in the gradual accumulation of binucleated cells (Fig. 4I). No sign of DNA condensation or cell cleavage was observed in these binucleated cells (data not shown), strongly suggesting that inhibition of YY1 function results in cytokinesis failure.

Identification of YY1 target genes in primary cells. While a substantial body of studies established a role for YY1 in transcriptional regulation, most YY1-responsive genes identified so far have yet to be validated as bona fide YY1 target genes in vivo. To gain mechanistic insights into YY1 developmental and cellular functions, we used a genomewide approach to identify YY1 target genes in mouse embryonic fibroblasts. Microarray analysis performed on $yy1^{+/+}$ and $yy1^{flox/-}$ MEFs (expressing ~25% of the normal complement of YY1) allowed us to identify 524 genes whose expression was affected by a reduction of the YY1 level. The complete list of YY1-responsive genes is provided in Table S1 in the supplemental material, and the target genes whose functions are the most relevant to the phenotypes described in this study are presented in Table 2. It is worth mentioning that approximately 90% of the genes affected by partial depletion of YY1 were found to display similar (i.e., comparable or more pronounced) changes in their expression profiles after complete depletion of YY1 in Cre-treated $yy1^{flox/-}$ MEFs (data not shown).

Consistent with the ability of YY1 to act as a transcriptional activator and a transcriptional repressor, inhibition of YY1 function led to up-regulation of 231 genes and down-regulation of 293 genes. In addition to key regulators of cell cycle progression, various genes involved in cytokinesis, mitosis, DNA replication, and apoptosis were also affected. YY1 depletion also led to the deregulation of a plethora of genes involved in various aspects of cellular functions such as cell survival, growth, and proliferation; oncogenic transformation; cell adhesion/migration; cytoskeleton biogenesis and organization; DNA repair; transcription; and epigenetic regulation of gene expression, metabolism, and signal transduction. Consistent with its essential role during development, YY1 depletion affected the expression of various genes required for cellular differentiation, embryonic patterning, and morphogenesis. Finally, genes required for homeostasis, DNA repair, and stress and immune responses were found among the most-represented functional groups, suggesting that YY1 might influence a broad spectrum of biological processes through a diverse and complex network of transcriptional changes.

To confirm the microarray data, the expression of 22 putative YY1 target genes was analyzed by RT-PCR in untreated $yy1^{+/+}$ and $yy1^{flox/-}$ MEFs (Fig. 5A). A similar approach was used to investigate the effects of complete depletion of YY1 on the expression of 21 of these putative targets in Cre-treated $yy1^{+/+}$ and $yy1^{f/f}$ MEFs (Fig. 5B). Among the candidates analyzed were the genes for cell cycle regulators *p21*, *p57*, *cdc46*/*mcm5*, *polα1*, *cyclin B1* and *cyclin B2*, known regulators of mitosis and cytokinesis (*Incenp*, *CenpA*, *Plk1*, *Birc-5*/*Survivin*, and *Cap-d2*), and epigenetic regulators of mammalian development (*Suv39h2* and *Dnmt3a*). The p53 target genes *Mdm2*, *Sip27*, *Gadd45γ*, *Dda3*, and *Perp* were selected due to their involvement in p53-dependent regulation of the cell cycle and apoptosis. Several genes involved in the regulation of cell survival, growth, and differentiation during development (e.g., *Bdnf*, *Ntf3*, *Nsg1*, *Tgfβ2*, and *Btg2*), as well as a few other genes (*BM88*, *Hmgb3*, *Nisnap1*, and *Sfxn1*) regulating diverse biological processes, were also studied. The expression of all candidate target genes tested was found to be affected by partial (Fig. 5A) and/or complete (Fig. 5B) depletion of YY1, as predicted based on the microarray results (Table 2; see also Table S1 in the supplemental material).

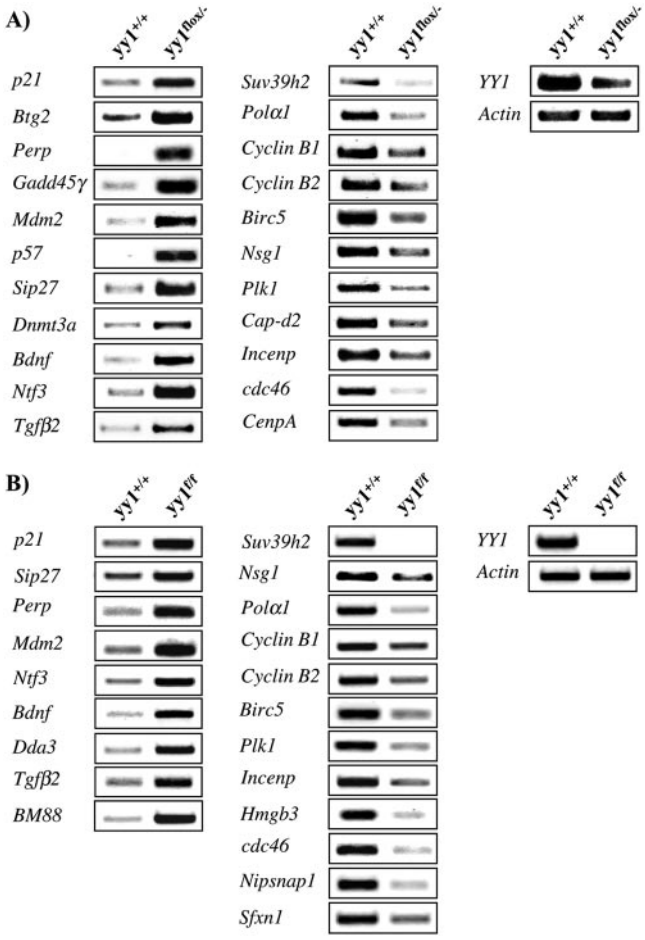

FIG. 5. Confirmation of potential targets of YY1 by semiquantitative RT-PCR. (A) Validation of the microarray data in $yy1^{flox/-}$ MEFs. Eleven genes whose expression was higher in the $yy1^{flox/-}$ MEFs than in their wild-type ($yy1^{+/+}$) counterparts (Table 2 and Table 1 in the supplemental material) were selected for RT-PCR analysis using RNAs extracted from untreated $yy1^{+/+}$ and $yy1^{flox/-}$ MEFs 4 days postisolation (left panel). Eleven genes expected to be down-regulated in the mutant cells were also analyzed (middle panel). (B) Deregulation of putative YY1 target genes upon complete depletion of YY1 in MEFs. Nine genes whose expression was induced by partial depletion of YY1 (i.e., untreated $yy1^{flox/-}$ MEFs) were selected for RT-PCR analysis performed on RNAs isolated from Cre-treated $yy1^{+/+}$ and $yy1^{f/f}$ MEFs at 6 days posttreatment (left panel). The expression of 12 genes expected to be down-regulated upon partial depletion of YY1 was also analyzed (middle panel). In both panels A and B, the YY1 and actin control RT-PCRs are shown in the right panels.

Depletion of YY1 does not lead to p53 induction in primary cells. We and others have previously shown that, in some cellular contexts, ablation of YY1 results in elevated levels of the tumor suppressor p53 and subsequent activation of p53-

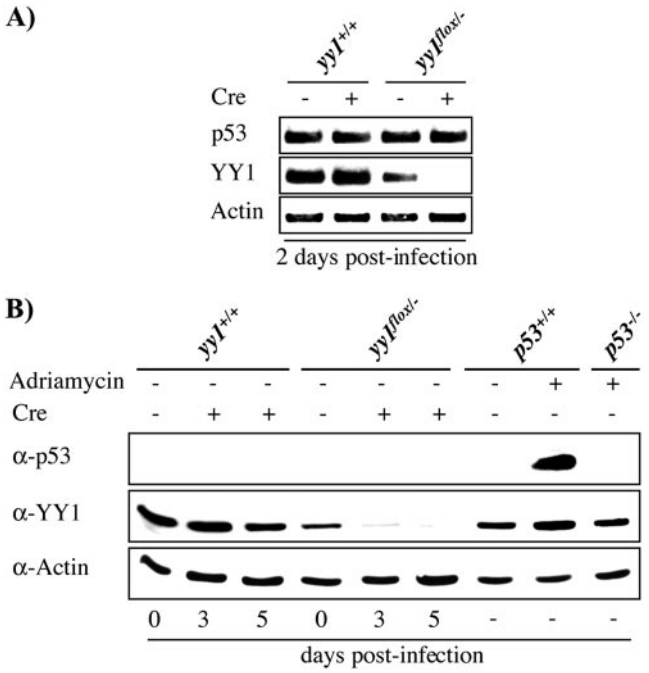

FIG. 6. Depletion of YY1 does not affect p53 expression in MEFs. (A) RT-PCR analysis of p53 mRNA level in MEFs isolated from $yy1^{flox/-}$ mice and their wild-type ($yy1^{+/+}$) littermates 2 days postinfection with adenovirus-Cre (i.e., 4 days postisolation). The YY1 and actin RT-PCRs are shown as controls. (B) Western blot analysis of p53 protein levels in $yy1^{flox/-}$ and $yy1^{+/+}$ MEFs was performed at various time points postinfection with adenovirus-Cre, using an anti-p53 antibody (PAB240). Adriamycin treatment (2 μg/ml for 10 h) of wild-type ($p53^{+/+}$) and p53 null ($p53^{-/-}$) MEFs was used as a control. Equal loading of the protein extracts and Cre-mediated depletion of YY1 were ensured by using antiactin (MAB1501) and anti-YY1 (H414) antibodies, respectively.

dependent pathways controlling cell growth and/or apoptosis (5, 26, 65). Strikingly, analysis of the microarray data revealed that approximately 40 YY1-responsive genes have previously been identified as p53 target genes (18, 27, 31, 40, 42, 74), their deregulation upon depletion of YY1 mimicking the effects of p53 induction (see Table 2; see also Table S1 in the supplemental material). Taken together, these results raise the possibility that the cellular phenotype (i.e., cell cycle arrest) and changes in gene expression profiles induced by depletion of YY1 in mouse embryonic fibroblasts might be mediated, at least in part, via an increase in p53 expression and/or stability.

To investigate this hypothesis, we analyzed the effects of YY1 depletion on the cellular levels of p53 mRNA and protein (Fig. 6). Consistent with our microarray data (see Table S1 in the supplemental material, and data not shown), we did not observe any significant effect of partial (i.e., untreated $yy1^{flox/-}$ MEFs) or complete (i.e., Cre-treated $yy1^{flox/-}$ MEFs) depletion of YY1 on p53 mRNA levels (Fig. 6A). While a strong increase in p53 protein level was observed in adriamycin-treated wild-type MEFs (used as a positive control for p53 induction), Western blot analysis showed that YY1 depletion did not affect the steady-state level of p53 protein in $yy1^{flox/-}$ MEFs (Fig. 6B). Consistently, no significant fluctuations of p53 mRNA and protein levels were detected after complete depletion of YY1 in $yy1^{f/f}$ MEFs (data not shown).Together, these results strongly suggest that the cellular phenotype and molecular targets induced by depletion of YY1 in MEFs are unlikely to result from induction of p53.

Depletion of YY1 inhibits cell proliferation and cytokinesis in HeLa cells. In order to circumvent some of the limitations associated with mouse embryonic fibroblasts and confirm our results in a different cellular context, we investigated the effect of RNAi-mediated inhibition of YY1 in HeLa cells, in which p53 is inactivated by the human papillomavirus oncoprotein E6.

The effects of YY1 depletion on cell viability and proliferation were assessed by a colony-forming assay (Fig. 7B) and FACS analysis (Fig. 7C), performed after transfection with a control or YY1 RNAi vector and subsequent selection of the transfected cells. Under these conditions, the YY1 protein level was dramatically reduced upon transfection of the YY1 RNAi vector (Fig. 7A). We found that the number and size of cell colonies formed by the RNAi-depleted cells were greatly reduced compared to those of mock-transfected cells (Fig. 7B). This is consistent with the phenotype resulting from complete depletion of YY1 in mouse primary cells (Fig. 4D and E, Cre-treated $yy1^{flox/-}$ and $yy1^{f/f}$ MEFs) and reinforces the idea that YY1 is required for cell survival and/or cell proliferation.

Microscopic observation of the cells (see below), Western blot analysis of PARP cleavage (a marker of apoptotic cell death; see Fig. 8), as well as FACS analysis (Fig. 7C) did not reveal any sign of apoptosis in the RNAi-treated cells. Although inhibition of YY1 function also resulted in the appearance of a small fraction of polyploid cells (i.e., cells having a DNA content higher than 4N), the most dramatic effect of YY1 RNAi on the cell cycle profile was a pronounced accumulation of cells having a 4N DNA content (Fig. 7C). Based on FACS analysis of three independent experiments, the percentage of tetraploid cells in the control and YY1 RNAi cell populations was estimated to be 24.7% ± 1.8% and 43.2% ± 1%, respectively.

To characterize the proliferative arrest caused by depletion of YY1 in more detail, we examined the cellular and nuclear morphology of the YY1-depleted cells by phase-contrast light microscopy (data not shown) and fluorescence microscopy after DAPI staining (Fig. 7D to F). Costaining of the control and YY1 RNAi-treated cells with anti-YY1 and antitubulin antibodies revealed that most cells affected by the YY1 RNAi had nuclei with uncondensed chromosomes, excluding mitotic arrest as the cause of the accumulation of the tetraploid cells (data not shown; see Fig. 7E). The most striking effect induced by inhibition of YY1 function was the gradual accumulation of cells containing more than one nucleus and/or displaying various other types of nuclear abnormalities (Fig. 7D).

As shown in Fig. 7E, the majority of YY1-negative cells (i.e., in which YY1 nuclear staining was extremely low or undetectable) containing more than one nucleus were binucleated and showed no detectable sign of DNA condensation or cell cleavage. Only a very small percentage of YY1-negative cells accumulated more than two nuclei (Fig. 7E and data not shown). The YY1-RNAi treated cells also displayed other nuclear anomalies, including deformed or bilobed nuclei, micronuclei, and DNA bridges, with a high frequency (Fig. 7D and F). Besides these alterations of their nuclear morphology, we found that most cells affected by the YY1 RNAi were abnor-

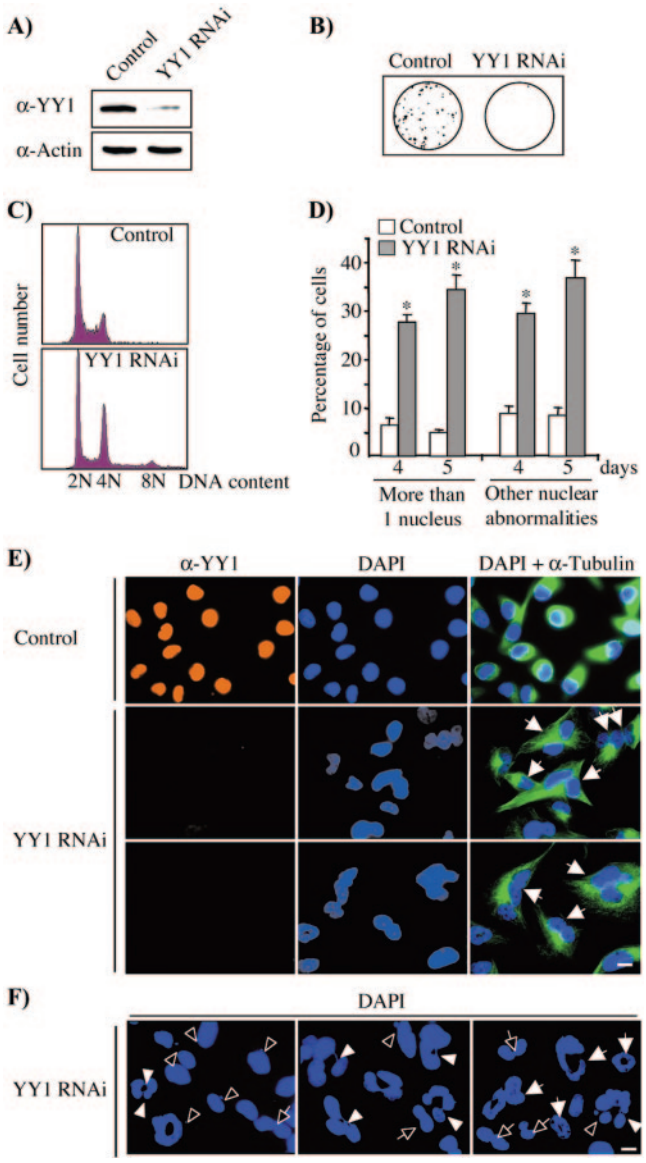

FIG. 7. Depletion of YY1 induces proliferation and cytokinesis defects in HeLa cells. (A) Efficient depletion of YY1 after RNAi in HeLa cells. After cotransfection of a control or YY1 RNAi plasmid with a puromycin resistance-encoding vector, the transfected cells were selected by puromycin treatment, and the expression level of YY1 was assessed by Western blot using an anti-YY1 antibody (H414). Equal loading of the protein extracts was confirmed using a monoclonal antiactin (MAB1501) antibody. (B) Effect of YY1 depletion on cell proliferation. HeLa cells were cotransfected and selected as in panel A, and their growth properties were analyzed by the colony-forming assay. (C) Cell cycle profile induced by depletion of YY1. FACS analysis was performed on HeLa cells cotransfected and selected (as described for panel A) 4 days after transfection with the RNAi plasmids. (D to F) Cytokinesis defects and nuclear abnormalities induced by depletion of YY1. HeLa cells transfected with a control or a YY1 RNAi plasmid were plated on coverslips and analyzed by immunofluorescence using an anti-YY1 antibody (H414; red), DAPI to stain the DNA (blue), and an antibody directed against α-tubulin (B512; green). Representative pictures are shown in panel E, and cells displaying more than one nucleus are indicated by solid arrows. Examples of the nuclear abnormalities induced by inhibition of YY1 (scored as other nuclear abnormalities in panel D) are shown in panel F. These nuclear defects include micronuclei (open arrowheads), DNA bridges (solid arrowheads), bilobed and dumbbell-shaped nuclei (open arrows), and other alterations of the nuclear morphology (solid arrows). Note that this panel is a montage generated by selecting only YY1-negative cells displaying nuclear anomalies. In panels E and F, the bar corresponds to 10 μm. The percentages of cells with more than one nucleus or with nuclear abnormalities were determined 4 and 5 days posttransfection. The results are shown in panel D and correspond to the mean ± standard deviation of three values obtained in independent experiments. Within each experiment, at least 500 cells per sample were scored, with only YY1-negative cells being analyzed in the YY1 RNAi samples. *, $P < 0.001$, YY1 RNAi versus the control (Student's t test).

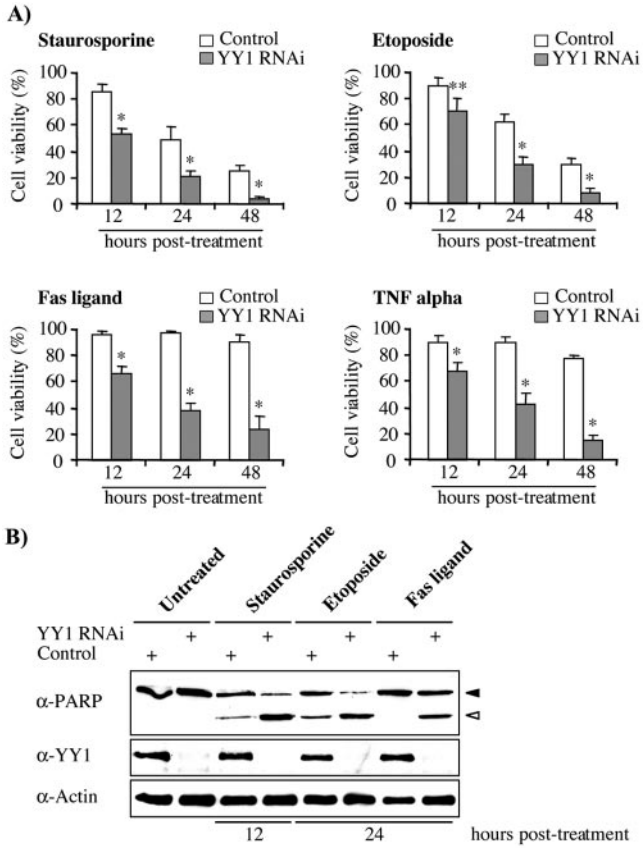

FIG. 8. RNAi-mediated depletion of YY1 sensitizes HeLa cells to various apoptotic agents. Puromycin-selected HeLa cells were treated with various apoptotic agents (200 nM of staurosporine, 100 μM of etoposide, 100 ng/ml of Fas ligand, and 10 ng/ml of tumor necrosis factor [TNF] alpha) 4 days after transfection of the control and YY1 RNAi vectors. Cell viability (A) and cell death (B) were then quantified at various time points posttreatment. The results shown in panel A correspond to the mean ± standard deviation of three values obtained in independent transfections, the number of viable cells in the treated control and YY1 RNAi cell populations being expressed as a percentage of that observed in the corresponding untreated samples harvested at the same time points. *, $P < 0.01$, YY1 RNAi versus control cells; **, $P < 0.05$, YY1 RNAi versus control cells (Student's t test). Western blot analysis of PARP cleavage was used to determine apoptotic cell death (panel B); full-length PARP and cleavage fragment are indicated by a solid and an open arrowhead, respectively. Efficient depletion of YY1 upon transfection of the RNAi plasmid and equal loading of the total cell extracts were ensured by using anti-YY1 (H10) and antiactin (MAB1501) antibodies.

mally flat and large compared to the control cells, and the size of their nucleus was also increased (Fig. 7E and F, and data not shown). Thus, the phenotype induced by depletion of YY1 in HeLa cells is essentially identical to that observed in mouse

TABLE 3. Effect of YY1 depletion on cell cycle progression in HeLa cells[a]

RNAi	Mean % of cells ± SD			
	G_1	S	G_2/early M (pro- to anaphase)	Late M/cytokinesis (ana- to telophase)
Control	22.1 ± 1.9	41 ± 1.7	29.7 ± 0.9	7.2 ± 1.2
YY1	25.8 ± 0.2	45.5 ± 1.3	26.5 ± 1.1	2.1 ± 0.2

[a] HeLa cells were transfected with a control or YY1 RNAi plasmid and stained with antibodies directed against PCNA (S phase), cyclin B1 (G_2/early M phases), and α-tubulin (midbody/cytokinesis). Costaining with an anti-YY1 antibody was performed to identify YY1-negative cells. The percentages of cells in G_1, S, G_2/early M, and late M/cytokinesis phases were determined 5 days post-transfection. The results are expressed as the mean ± standard deviation of three values obtained in independent experiments. In each experiment, at least 500 cells were counted, with only YY1-negative cells being scored in the YY1 RNAi samples.

primary cells (Fig. 4) and strongly suggests that inhibition of YY1 induces cytokinesis failure.

To gain further insights into the molecular mechanisms underlying the role of YY1 in the regulation of cell cycle progression and cell ploidy, we examined the expression of various markers specific to the different phases of the cell cycle (Fig. S2 and S3 in the supplemental material). Based on these stainings, the percentages of cells in G_1, S, G_2/early M (i.e., prophase-end of metaphase), and late M/cytokinesis (i.e., anaphase-telophase) phases in the control and YY1 RNAi cell populations were determined (Table 3).

YY1 RNAi did not significantly affect the percentage of G_2 cells (data not shown) or G_2/early M cells (Table 3). In contrast, inhibition of YY1 function led to a pronounced diminution of the percentage of cells undergoing cytokinesis during late M phase (Table 3). We did not observe any significant increase in the percentage of G_1 cells in the YY1 RNAi samples, arguing against a G_1 cell cycle arrest. Similarly, depletion of YY1 did not significantly affect the percentage of cells in S phase, strongly suggesting that a significant number of the binucleated cells (representing ~35% of the YY1-depleted cells) were undergoing DNA replication.

Considering exclusively YY1-negative cells containing more than one nucleus, we determined that 44% ± 3% of such cells contained PCNA-positive DNA replication foci. Consistently, a significant number of binucleated YY1-negative cells (24.3% ± 1%) were found to be in G_2 phase (see also Fig. S2 in the supplemental material). Based on these immunostaining experiments, we conclude that (i) the proliferation defects and accumulation of tetraploid cells induced by depletion of YY1 do not result from a blockage at the G_2/M transition, (ii) depletion of YY1 impairs cytokinesis initiation, leading to the accumulation of cells containing two nuclei, and (iii) binucleated cells do not undergo cell cycle arrest immediately after cytokinesis failure, but instead progress through the next G_1 phase and subsequently undergo at least one round of illegitimate DNA replication leading to polyploidization. The small percentage of YY1-negative cells displaying more than two nuclei strongly suggests that most binucleated cells cannot proceed to the next round of mitosis, but rather undergo cell cycle arrest. Supporting this view, the percentage of YY1-negative cells initiating mitosis (i.e., cells in early M phase) decreased slowly but gradually throughout the course of the experiment, while the percentage of control cells undergoing mitosis was not significantly affected (data not shown).

Taken together, these results demonstrate that complete inhibition of YY1 function results in cytokinesis failure and induces severe cell proliferation defects, uncovering new p53-independent functions of YY1-mediated regulation of cell cycle progression.

Depletion of YY1 sensitizes HeLa cells to various apoptosis-inducing agents. Inhibition of YY1 function has previously been shown to modulate the cellular sensitivity to p53-mediated apoptosis in response to DNA damage (26). In the present study, we report that depletion of YY1 leads to a deregulation of several apoptosis-related genes without any significant effect on p53 levels (Table 2 and Fig. 6). These observations led us to investigate the potential direct involvement of YY1 in the regulation of apoptotic programs. Therefore, we analyzed the effects of YY1 depletion on the cellular response of HeLa cells, which lack functional p53, to various DNA-damaging and nondamaging apoptotic inducers.

As shown in Fig. 8, puromycin-selected HeLa cells transfected with the control or YY1 RNAi were treated with known activators of mitochondrion-dependent apoptotic pathways (i.e., staurosporine and etoposide) and of the death receptor-dependent pathways (i.e., tumor necrosis factor and Fas ligand). After ensuring efficient depletion of YY1 in the YY1 RNAi-treated cells (Fig. 8B), we quantified cell viability (Fig. 8A) and cell death (using PARP cleavage as a marker of apoptotic cell death; Fig. 8B) in the untreated and treated control and YY1 RNAi cell populations. Consistent with our previous observations (see above), RNAi-mediated inhibition of YY1 in HeLa cells did not trigger apoptosis in the absence of any apoptotic agents (Fig. 8B, and data not shown). However, depletion of YY1 dramatically increased the cellular sensitivity to all apoptotic agents tested. Indeed, treatment with staurosporine, etoposide, tumor necrosis factor, and Fas ligand led to a much greater decrease in the number of viable cells in the YY1 RNAi cell population than in the control cell population (Fig. 8A).

Consistently, treatment of the YY1-depleted cells with staurosporine, etoposide, and Fas ligand led to a marked increase in PARP cleavage, this effect being much more pronounced than that observed upon treatment of the control cells (Fig. 8B). Taken together with previous results showing that YY1 inhibits genotoxic stress-induced activation of p53 (26), our data strongly suggest that YY1 plays important roles in the regulation of multiple p53-dependent as well as p53-independent pathways mediating programmed cell death in response to a broad spectrum of apoptotic agents.

DISCUSSION

In this study, we used conditional gene targeting to investigate the developmental, cellular, and molecular functions of the transcription factor YY1 during mouse embryogenesis and in cultured primary cells. Taking advantage of a *yy1* hypomorphic allele, we demonstrate the essential dosage-dependent requirement for YY1 in late embryogenesis. Indeed, while mice expressing ~75% of the normal level of YY1 are viable and do not display any obvious developmental defects, reduction of the YY1 protein level by ~50% induces lethality in a

small subset of mice and affects embryonic growth. Further diminution of the YY1 level significantly increases the penetrance of the growth retardation and embryo-lethal phenotype. Approximately half of the mice expressing ~25% of normal YY1 levels died during late embryogenesis, a developmental period during which active morphogenesis and organogenesis are occurring. Thus, the phenotype of mice expressing ~25% of normal YY1 levels differs dramatically from that of *yy1* null embryos, which die around the time of implantation, a stage characterized by intense cell proliferation (20). These observations suggest that ~25% of the normal YY1 level can support cellular proliferation, at least to some extent, while complete depletion of YY1 cannot, which is consistent with the dose-dependent growth suppressor effect of YY1 observed in cultured embryonic fibroblasts (see below).

Approximately half of the mice expressing ~25% of the normal complement of YY1 developed and survived until birth but died shortly thereafter from respiratory failure. While histological examination demonstrated that the lung alveoli were collapsed, electronic microscopy did not reveal any major ultrastructural defects. In particular, alveolar type II cells, which are responsible for the synthesis of lung surfactant, appeared normal (data not shown), suggesting that the respiratory failure induced by depletion of YY1 results from developmental defects affecting organs other than the lung. Interestingly, inactivation of several of the novel YY1 target genes identified here (including *lamin B1*, *Bdnf*, the transcription factor *FoxM1*, and the cell cycle regulator *p57*) impairs the development of various tissues and causes respiratory failure (30, 32, 67, 73, 81).

Functional defects of the respiratory musculature, of its motor innervation, as well as of the central control center (i.e., respiratory rhythm-generating neurons) have been shown to cause respiratory failure. In this regard, it is worth pointing out that a large number of muscle-specific genes were derepressed after depletion of YY1 in MEFs (including various myosin-, procollagen-, troponin-, and actin-encoding genes [Table 2; see also Table S1 in the supplemental material]). Importantly, YY1 was recently shown to recruit HDAC1 as well as the polycomb group protein EZH2 (enhancer of zeste homolog 2), a histone H3 methyltransferase whose activity is associated with stable transcriptional repression, to genomic regions of silent muscle-specific loci in undifferentiated myoblasts (17). Polycomb group proteins play important roles in long-term, inheritable gene silencing required for maintenance of cell identity during development and differentiation. However, the mechanisms underlying the recruitment of polycomb group protein complexes to their molecular targets as well as the identity of these targets remain largely unknown. It would be extremely interesting to investigate the possibility that YY1 might target HDACs and/or polycomb group protein-containing complexes to specific DNA recognition sites within the regulatory regions of its target genes and induce stable transcriptional repression of muscle-specific genes in undifferentiated muscle progenitor cells and differentiated nonmuscle cells.

Strikingly, depletion of YY1 in embryonic fibroblasts also led to the activation of various genes whose expression and function are normally restricted to neuronal cells, including the neuronal survival and plasticity factors neurotrophin 3 (*Ntf3*) and brain-derived neurotrophic factor (*Bdnf*), the imprinted gene neuronatin, and the brain-specific helix-loop-helix proteins encoded by *Neurod6* (neurogenic differentiation 6), *BM88*, and several others. Although YY1 might directly repress some neuron-specific genes, the observation that YY1 depletion dramatically inhibits the expression of REST (repressor element 1 silencing transcription factor [Table 2]) in MEFs suggests alternative regulatory mechanisms.

Several studies demonstrated that the transcriptional repressor REST plays essential roles in restricting expression of neuronal genes to neurons by mediating active repression as well as long-term epigenetic silencing of these genes in differentiated nonneuronal cells (6, 8, 19, 29, 38, 43, 49, 50, 54, 55). Importantly, REST is highly expressed in pluripotent cells, in which it also represses neuron-specific gene expression, but is dramatically down-regulated during the transition to lineage-restricted neural progenitors, completely disappearing as progenitors exit the cell cycle and differentiate into mature neurons (7, 54). It is thus conceivable that YY1 might, directly or via the modulation of REST expression, participate in the maintenance of nonneuronal cell identity by contributing to neuron-specific gene silencing in such cells and/or play a role in the acquisition of neuronal traits in differentiating neuronal precursors. It would be extremely interesting to study YY1 expression during neuronal cell specification and differentiation and take advantage of our conditional knockout mice to investigate its role during neurogenesis.

While YY1 target genes are likely to play crucial roles in its developmental functions, various YY1-binding partners could also contribute to its biological activities. In this regard, it is interesting that abrogation of the acetyltransferase activity of p300, which acetylates YY1 and modulates its activity (34, 80), also causes neonatal lethality due to respiratory failure in mice (61). In addition, constitutive inactivation of p300 in mice reveals important dosage-dependent effects on cell proliferation, embryonic growth, and viability, as well as a partially penetrant neural tube closure defect similar to that displayed by a subset of heterozygous ($yy1^{+/-}$) and compound heterozygous ($yy1^{flox/-}$) mutant mice (20, 79) (data not shown). These phenotypic similarities suggest that YY1-p300 functional interplay could play an important role during development. Further analysis will be required to decipher the mechanisms underlying YY1 developmental functions and determine the contributions of its target genes and interacting partners.

Analysis of the cellular phenotypes induced by partial and complete depletion of YY1 in MEF cells (Fig. 4) allowed us to demonstrate that YY1 regulates cell proliferation in a dose-dependent manner. Interestingly, while the growth properties of MEFs expressing ~50% and ~25% of the normal complement of YY1 were indisputably impaired, these cells kept proliferating at a slow but steady rate. In contrast, complete depletion of YY1 in primary and tumor cells induced proliferative arrest (Fig. 4 and 7). In addition, loss of YY1 function resulted in cytokinesis failure in both embryonic fibroblasts (Fig. 4) and HeLa cells (Fig. 7), but no significant accumulation of binucleated cells was observed in untreated $yy1^{flox/-}$ MEFs expressing ~25% of the normal complement of YY1 (data not shown). Taken together, theses results strongly suggest that partial depletion of YY1 impairs cell proliferation by inducing an extension of the cell cycle phases, while complete

loss of YY1 blocks cell cycle progression and leads to cell cycle arrest.

Consistently, genome-wide gene expression analysis revealed that various cell cycle-related genes were deregulated upon depletion of YY1 (Table 2; see also Table S1 in the supplemental material). Interestingly, a large number of YY1-responsive genes involved in cell cycle control have previously been shown to be regulated by E2F transcription factors (13, 46). Among these YY1- and E2F-regulated genes are *p21*, cyclin A2, *mcmd4-7*, *polα1*, polo-like kinase, and aurora kinase B, as well as various other checkpoint regulators (including *Bub1*, *Bub1b*, *Mad2*, and *CenpE*). Supporting the hypothesis that YY1 might share common functions and/or molecular targets with E2Fs, coincident binding of YY1 and E2F2 or E2F3 on adjacent recognition sites within the *cdc6* promoter results in synergistic activation of this promoter (53). As several other YY1 and/or E2F target genes contain binding sites for both transcription factors (Y. Shi, unpublished observations) (53), this mechanism might provide a molecular basis for the specificity of E2F functions as well as for YY1 in cell cycle control.

Consistent with the novel and unanticipated function for YY1 in cytokinesis uncovered in this study, several known key regulators of mitosis and cytokinesis, such as survivin/Birc5, polo-like kinase, inner centromere protein, aurora kinases A and B, and various others (Table 2), were found to be deregulated by depletion of YY1. Interestingly, RNAi-mediated inhibition of survivin, the expression of which is significantly down-regulated upon depletion of YY1, impairs cytokinesis and cell proliferation (78). Inactivation of survivin was shown to induce p53 up-regulation and subsequent activation of a p53- and p21-dependent checkpoint, resulting in cell cycle arrest in G_1 phase (78). Despite contradictory reports, other studies support the hypothesis that cytokinesis failure activates a tetraploidy checkpoint response blocking cell cycle progression in G_1 phase (1, 63, 69, 70, 75).

Several lines of evidence argue against the cell cycle arrest induced by complete depletion of YY1 being the result of the activation of such a checkpoint response. Indeed, we did not detect any significant effect of YY1 depletion on p53 levels in MEFs (Fig. 6), which, together with the previous demonstration that YY1 negatively regulates p53 stability in other cellular contexts (5, 26, 65), suggests that YY1-mediated regulation of p53 might be cell type and/or species specific. Consistent with the observation that depletion of YY1 does not affect steady-state p53 levels in MEFs, RNAi-mediated inhibition of YY1 function was found to induce proliferative arrest in *p53* null mouse embryonic fibroblasts (Y. Shi, unpublished observation). In addition, inhibition of YY1 expression in HeLa cells, in which p53 is inactivated by the papillomavirus oncoprotein E6, also resulted in cell cycle arrest and cytokinesis failure.

Immunostaining of HeLa cells allowed us to demonstrate that binucleated cells did not undergo cell cycle arrest immediately after cytokinesis failure, but progressed through the next G_1 phase and underwent at least one round of DNA endoreplication before exiting the cell cycle (see Fig. S2 and S3 in the supplemental material). Similarly, a significant fraction of YY1-depleted binucleated MEFs were found to undergo DNA replication, as indicated by their ability to incorporate bromodeoxyuridine (data not shown). Further strengthening the idea that YY1 ablation does not trigger activation of a p53- and p21-dependent tetraploidy checkpoint response, genetic rescue experiments demonstrated that YY1 depletion induced similar defects regardless of the status of *p21*. Indeed, no significant differences in growth properties or binucleated cell numbers were observed when comparing the effects of YY1 depletion in $p21^{+/+}$ versus *p21* null MEFs (see Fig. S4 in the supplemental material; also data not shown). Together, these data demonstrate that the effects of YY1 on cell cycle progression and cell proliferation are essentially p53 and p21 independent.

Despite the strong evidence that the effects of YY1 depletion on cell cycle progression and cell proliferation reported here are essentially p53 independent, we identified approximately 40 YY1-responsive genes that are known p53 targets (18, 27, 31, 40, 42, 74), suggesting that YY1 and p53 might directly regulate a common subset of related target genes in an antagonistic manner. While further analysis will be required to validate this hypothesis, it is supported by the recent finding that YY1 inhibits p53-mediated activation of *p21* and *Gadd45*, through a mechanism involving competitive binding for overlapping DNA recognition sites within these promoters (77). Together with the transcription-independent cross talk between these two transcription factors (26, 65), such convergence of YY1 and p53 on shared molecular targets could contribute to their antagonistic effects on cell growth and apoptosis.

Interestingly, depletion of YY1 results in the derepression of several proapoptotic genes (Table 2), including known p53 target genes (18, 27, 31, 40, 42, 74). YY1 has previously been shown to modulate p53-dependent apoptotic programs induced by genotoxic stress (26). Here, we report that depletion of YY1 increases the sensitivity of cells lacking p53 activity to various DNA-damaging and nondamaging apoptosis inducers. Indeed, inhibition of YY1 was found to sensitize tumor cells to etoposide, a chemotherapeutic agent used to treat a wide spectrum of human cancers, and to staurosporine; both of these activate mitochondrion-dependent apoptotic pathways. In addition, YY1-depleted cells were also more sensitive to tumor necrosis factor and Fas ligand-induced apoptosis, mediated through death receptor-dependent pathways. This finding is consistent with the observation that expression of Fas receptor (*Fas*) is derepressed upon inhibition of YY1 (Table 2).

While this work was in preparation, Vega et al. reported that rituximab, a chimeric anti-CD20 antibody used in the treatment of B non-Hodgkin's lymphoma, up-regulates Fas expression and sensitizes Fas-resistant tumor cells to Fas ligand-induced apoptosis by modulating YY1 expression and activity (71, 72). Therefore, through its ability to modulate the sensitivity of various tumor cell types to a broad spectrum of apoptotic agents inducing p53-dependent as well as p53-independent pathways, YY1 might be an attractive therapeutic target for cancer.

Together, our data uncovered important dosage-dependent functions of the transcription factor YY1 in embryonic growth and development, cell proliferation, cytokinesis, and apoptosis. Moreover, genome-wide analysis allowed us to identify over 500 putative YY1 target genes. The large number of YY1-responsive genes identified in this study is not surprising, as it

reflects the effects of YY1 removal on its direct targets as well as cascades of secondary events. Kinetic analysis of YY1-mediated transcriptional activation and repression combined with bioinformatic and chromatin immunoprecipitation approaches will allow us to distinguish direct versus indirect targets and characterize the histone modification profiles and cofactor recruitment induced by YY1. The findings presented here shed new light on the nature of the genetic programs and molecular mechanisms underlying YY1's biological activities.

ACKNOWLEDGMENTS

We thank Grace Gill (Harvard Medical School, Boston) for critical reading of the manuscript and helpful comments. We are extremely grateful to Shidong Jia and Thomas Roberts (Dana Farber Cancer Institute, Boston) for assistance during the genome-wide gene expression profiling analysis, which was performed at the Dana-Farber Microarray Core Facility. We also thank Roderick Bronson (Harvard Medical School, Boston) for histological analysis of the compound mutant mice.

El Bachir Affar and Frédérique Gay were fellowship recipients from the Taplin Funds for Discovery. Yujiang Shi and Maite Huarte were supported by fellowships from the NIH (F32GM070690) and from the Fundación Ramón Areces, respectively. This work was supported by a grant from the National Institutes of Health (GM53874) to Yang Shi.

REFERENCES

1. **Andreassen, P. R., F. B. Lacroix, O. D. Lohez, and R. L. Margolis.** 2001. Neither p21WAF1 nor 14-3-3sigma prevents G2 progression to mitotic catastrophe in human colon carcinoma cells after DNA damage, but p21WAF1 induces stable G1 arrest in resulting tetraploid cells. Cancer Res. **61:**7660–7668.
2. **Atchison, L., A. Ghias, F. Wilkinson, N. Bonini, and M. L. Atchison.** 2003. Transcription factor YY1 functions as a PcG protein in vivo. EMBO J. **22:**1347–1358.
3. **Austen, M., C. Cerni, J. M. Luscher-Firzlaff, and B. Luscher.** 1998. YY1 can inhibit c-Myc function through a mechanism requiring DNA binding of YY1 but neither its transactivation domain nor direct interaction with c-Myc. Oncogene **17:**511–520.
4. **Austen, M., B. Luscher, and J. M. Luscher-Firzlaff.** 1997. Characterization of the transcriptional regulator YY1. The bipartite transactivation domain is independent of interaction with the TATA box-binding protein, transcription factor IIB, TAFII55, or cAMP-responsive element-binding protein (CPB)-binding protein. J. Biol. Chem. **272:**1709–1717.
5. **Bain, M., and J. Sinclair.** 2005. Targeted inhibition of the transcription factor YY1 in an embryonal carcinoma cell line results in retarded cell growth, elevated levels of p53 but no increase in apoptotic cell death. Eur. J. Cell Biol. **84:**543–553.
6. **Ballas, N., E. Battaglioli, F. Atouf, M. E. Andres, J. Chenoweth, M. E. Anderson, C. Burger, M. Moniwa, J. R. Davie, W. J. Bowers, H. J. Federoff, D. W. Rose, M. G. Rosenfeld, P. Brehm, and G. Mandel.** 2001. Regulation of neuronal traits by a novel transcriptional complex. Neuron **31:**353–365.
7. **Ballas, N., C. Grunseich, D. D. Lu, J. C. Speh, and G. Mandel.** 2005. REST and its corepressors mediate plasticity of neuronal gene chromatin throughout neurogenesis. Cell **121:**645–657.
8. **Battaglioli, E., M. E. Andres, D. W. Rose, J. G. Chenoweth, M. G. Rosenfeld, M. E. Anderson, and G. Mandel.** 2002. REST repression of neuronal genes requires components of the hSWI.SNF complex. J. Biol. Chem. **277:**41038–41045.
9. **Bauknecht, T., R. H. See, and Y. Shi.** 1996. A novel C/EBPβ-YY1 complex controls the cell type-specific activity of the human papillomavirus type 18 upstream regulatory region. J. Virol. **70:**7695–7705.
10. **Baumeister, P., S. Luo, W. C. Skarnes, G. Sui, E. Seto, Y. Shi, and A. S. Lee.** 2005. Endoplasmic reticulum stress induction of the Grp78/BiP promoter: activating mechanisms mediated by YY1 and its interactive chromatin modifiers. Mol. Cell. Biol. **25:**4529–4540.
11. **Begon, D. Y., L. Delacroix, D. Vernimmen, P. Jackers, and R. Winkler.** 2005. Yin Yang 1 cooperates with activator protein 2 to stimulate ERBB2 gene expression in mammary cancer cells. J. Biol. Chem. **280:**24428–24434.
12. **Bennett, M. K., T. T. Ngo, J. N. Athanikar, J. M. Rosenfeld, and T. F. Osborne.** 1999. Co-stimulation of promoter for low density lipoprotein receptor gene by sterol regulatory element-binding protein and Sp1 is specifically disrupted by the yin yang 1 protein. J. Biol. Chem. **274:**13025–13032.
13. **Blais, A., and B. D. Dynlacht.** 2004. Hitting their targets: an emerging picture of E2F and cell cycle control. Curr. Opin. Genet. Dev. **14:**527–532.
14. **Brankin, B., T. C. Skaar, M. Brotzman, B. Trock, and R. Clarke.** 1998. Autoantibodies to the nuclear phosphoprotein nucleophosmin in breast cancer patients. Cancer Epidemiol. Biomarkers Prev. **7:**1109–1115.
15. **Breen, T. R., and I. M. Duncan.** 1986. Maternal expression of genes that regulate the bithorax complex of Drosophila melanogaster. Dev. Biol. **118:**442–456.
16. **Brown, J. L., D. Mucci, M. Whiteley, M. L. Dirksen, and J. A. Kassis.** 1998. The Drosophila Polycomb group gene pleiohomeotic encodes a DNA binding protein with homology to the transcription factor YY1. Mol. Cell **1:**1057–1064.
17. **Caretti, G., M. Di Padova, B. Micales, G. E. Lyons, and V. Sartorelli.** 2004. The Polycomb Ezh2 methyltransferase regulates muscle gene expression and skeletal muscle differentiation. Genes Dev. **18:**2627–2638.
18. **Ceballos, E., M. J. Munoz-Alonso, B. Berwanger, J. C. Acosta, R. Hernandez, M. Krause, O. Hartmann, M. Eilers, and J. Leon.** 2005. Inhibitory effect of c-Myc on p53-induced apoptosis in leukemia cells. Microarray analysis reveals defective induction of p53 target genes and upregulation of chaperone genes. Oncogene **24:**4559–4571.
19. **Chong, J. A., J. Tapia-Ramirez, S. Kim, J. J. Toledo-Aral, Y. Zheng, M. C. Boutros, Y. M. Altshuller, M. A. Frohman, S. D. Kraner, and G. Mandel.** 1995. REST: a mammalian silencer protein that restricts sodium channel gene expression to neurons. Cell **80:**949–957.
20. **Donohoe, M. E., X. Zhang, L. McGinnis, J. Biggers, E. Li, and Y. Shi.** 1999. Targeted disruption of mouse Yin Yang 1 transcription factor results in peri-implantation lethality. Mol. Cell. Biol. **19:**7237–7244.
21. **Erkeland, S. J., M. Valkhof, C. Heijmans-Antonissen, R. Delwel, P. J. Valk, M. H. Hermans, and I. P. Touw.** 2003. The gene encoding the transcriptional regulator Yin Yang 1 (YY1) is a myeloid transforming gene interfering with neutrophilic differentiation. Blood **101:**1111–1117.
22. **Farley, F. W., P. Soriano, L. S. Steffen, and S. M. Dymecki.** 2000. Widespread recombinase expression using FLPeR (flipper) mice. Genesis **28:**106–110.
23. **Flanagan, J. R., K. G. Becker, D. L. Ennist, S. L. Gleason, P. H. Driggers, B. Z. Levi, E. Appella, and K. Ozato.** 1992. Cloning of a negative transcription factor that binds to the upstream conserved region of Moloney murine leukemia virus. Mol. Cell. Biol. **12:**38–44.
24. **Gehring, W. J.** 1970. A recessive lethal (l(4)29) with a homeotic effect in D. melanogaster. Drosophila Inf. Serv. **45:**103–104.
25. **Girton, J. R., and S. H. Jeon.** 1994. Novel embryonic and adult homeotic phenotypes are produced by pleiohomeotic mutations in Drosophila. Dev. Biol. **161:**393–407.
26. **Gronroos, E., A. A. Terentiev, T. Punga, and J. Ericsson.** 2004. YY1 inhibits the activation of the p53 tumor suppressor in response to genotoxic stress. Proc. Natl. Acad. Sci. USA **101:**12165–12170.
27. **Gu, J., L. Zhang, S. G. Swisher, J. Liu, J. A. Roth, and B. Fang.** 2004. Induction of p53-regulated genes in lung cancer cells: implications of the mechanism for adenoviral p53-mediated apoptosis. Oncogene **23:**1300–1307.
28. **Hariharan, N., D. E. Kelley, and R. P. Perry.** 1991. Delta, a transcription factor that binds to downstream elements in several polymerase II promoters, is a functionally versatile zinc finger protein. Proc. Natl. Acad. Sci. USA **88:**9799–9803.
29. **Jepsen, K., O. Hermanson, T. M. Onami, A. S. Gleiberman, V. Lunyak, R. J. McEvilly, R. Kurokawa, V. Kumar, F. Liu, E. Seto, S. M. Hedrick, G. Mandel, C. K. Glass, D. W. Rose, and M. G. Rosenfeld.** 2000. Combinatorial roles of the nuclear receptor corepressor in transcription and development. Cell **102:**753–763.
30. **Jones, K. R., I. Farinas, C. Backus, and L. F. Reichardt.** 1994. Targeted disruption of the BDNF gene perturbs brain and sensory neuron development but not motor neuron development. Cell **76:**989–999.
31. **Kannan, K., N. Amariglio, G. Rechavi, J. Jakob-Hirsch, I. Kela, N. Kaminski, G. Getz, E. Domany, and D. Givol.** 2001. DNA microarrays identification of primary and secondary target genes regulated by p53. Oncogene **20:**2225–2234.
32. **Korver, W., M. W. Schilham, P. Moerer, M. J. van den Hoff, K. Dam, W. H. Lamers, R. H. Medema, and H. Clevers.** 1998. Uncoupling of S phase and mitosis in cardiomyocytes and hepatocytes lacking the winged-helix transcription factor Trident. Curr. Biol. **8:**1327–1330.
33. **Kwon, H. J., and H. M. Chung.** 2003. Yin Yang 1, a vertebrate polycomb group gene, regulates antero-posterior neural patterning. Biochem. Biophys. Res. Commun. **306:**1008–1013.
34. **Lee, J. S., K. M. Galvin, R. H. See, R. Eckner, D. Livingston, E. Moran, and Y. Shi.** 1995. Relief of YY1 transcriptional repression by adenovirus E1A is mediated by E1A-associated protein p300. Genes Dev. **9:**1188–1198.
35. **Lee, J. S., K. M. Galvin, and Y. Shi.** 1993. Evidence for physical interaction between the zinc-finger transcription factors YY1 and Sp1. Proc. Natl. Acad. Sci. USA **90:**6145–6149.
36. **Lee, J. S., R. H. See, K. M. Galvin, J. Wang, and Y. Shi.** 1995. Functional interactions between YY1 and adenovirus E1A. Nucleic Acids Res. **23:**925–931.
37. **Li, E., T. H. Bestor, and R. Jaenisch.** 1992. Targeted mutation of the DNA methyltransferase gene results in embryonic lethality. Cell **69:**915–926.
38. **Lunyak, V. V., and M. G. Rosenfeld.** 2005. No rest for REST: REST/NRSF regulation of neurogenesis. Cell **121:**499–501.
39. **Meyers, E. N., M. Lewandoski, and G. R. Martin.** 1998. An Fgf8 mutant

allelic series generated by Cre- and Flp-mediated recombination. Nat. Genet. **18:**136–141.
40. **Mirza, A., Q. Wu, L. Wang, T. McClanahan, W. R. Bishop, F. Gheyas, W. Ding, B. Hutchins, T. Hockenberry, P. Kirschmeier, J. R. Greene, and S. Liu.** 2003. Global transcriptional program of p53 target genes during the process of apoptosis and cell cycle progression. Oncogene **22:**3645–3654.
41. **Mosmann, T.** 1983. Rapid colorimetric assay for cellular growth and survival: application to proliferation and cytotoxicity assays. J. Immunol. Methods **65:**55–63.
42. **Nakamura, Y.** 2004. Isolation of p53-target genes and their functional analysis. Cancer Sci. **95:**7–11.
43. **Naruse, Y., T. Aoki, T. Kojima, and N. Mori.** 1999. Neural restrictive silencer factor recruits mSin3 and histone deacetylase complex to repress neuron-specific target genes. Proc. Natl. Acad. Sci. USA **96:**13691–13696.
44. **Park, K., and M. L. Atchison.** 1991. Isolation of a candidate repressor/activator, NF-E1 (YY-1, delta), that binds to the immunoglobulin kappa 3′ enhancer and the immunoglobulin heavy-chain mu E1 site. Proc. Natl. Acad. Sci. USA **88:**9804–9808.
45. **Petkova, V., M. J. Romanowski, I. Sulijoadikusumo, D. Rohne, P. Kang, T. Shenk, and A. Usheva.** 2001. Interaction between YY1 and the retinoblastoma protein. Regulation of cell cycle progression in differentiated cells. J. Biol. Chem. **276:**7932–7936.
46. **Ren, B., H. Cam, Y. Takahashi, T. Volkert, J. Terragni, R. A. Young, and B. D. Dynlacht.** 2002. E2F integrates cell cycle progression with DNA repair, replication, and G_2/M checkpoints. Genes Dev. **16:**245–256.
47. **Rezai-Zadeh, N., X. Zhang, F. Namour, G. Fejer, Y. D. Wen, Y. L. Yao, I. Gyory, K. Wright, and E. Seto.** 2003. Targeted recruitment of a histone H4-specific methyltransferase by the transcription factor YY1. Genes Dev. **17:**1019–1029.
48. **Riggs, K. J., S. Saleque, K. K. Wong, K. T. Merrell, J. S. Lee, Y. Shi, and K. Calame.** 1993. Yin-yang 1 activates the c-*myc* promoter. Mol. Cell. Biol. **13:**7487–7495.
49. **Roopra, A., R. Qazi, B. Schoenike, T. J. Daley, and J. F. Morrison.** 2004. Localized domains of G9a-mediated histone methylation are required for silencing of neuronal genes. Mol. Cell **14:**727–738.
50. **Roopra, A., L. Sharling, I. C. Wood, T. Briggs, U. Bachfischer, A. J. Paquette, and N. J. Buckley.** 2000. Transcriptional repression by neuron-restrictive silencer factor is mediated via the Sin3-histone deacetylase complex. Mol. Cell. Biol. **20:**2147–2157.
51. **Satijn, D. P., K. M. Hamer, J. den Blaauwen, and A. P. Otte.** 2001. The polycomb group protein EED interacts with YY1, and both proteins induce neural tissue in *Xenopus* embryos. Mol. Cell. Biol. **21:**1360–1369.
52. **Sauer, B., and N. Henderson.** 1988. Site-specific DNA recombination in mammalian cells by the Cre recombinase of bacteriophage P1. Proc. Natl. Acad. Sci. USA **85:**5166–5170.
53. **Schlisio, S., T. Halperin, M. Vidal, and J. R. Nevins.** 2002. Interaction of YY1 with E2Fs, mediated by RYBP, provides a mechanism for specificity of E2F function. EMBO J. **21:**5775–5786.
54. **Schoenherr, C. J., and D. J. Anderson.** 1995. The neuron-restrictive silencer factor (NRSF): a coordinate repressor of multiple neuron-specific genes. Science **267:**1360–1363.
55. **Schoenherr, C. J., A. J. Paquette, and D. J. Anderson.** 1996. Identification of potential target genes for the neuron-restrictive silencer factor. Proc. Natl. Acad. Sci. USA **93:**9881–9886.
56. **Seligson, D., S. Horvath, S. Huerta-Yepez, S. Hanna, H. Garban, A. Roberts, T. Shi, X. Liu, D. Chia, L. Goodglick, and B. Bonavida.** 2005. Expression of transcription factor Yin Yang 1 in prostate cancer. Int. J. Oncol. **27:**131–141.
57. **Seto, E., B. Lewis, and T. Shenk.** 1993. Interaction between transcription factors Sp1 and YY1. Nature **365:**462–464.
58. **Shah, G. M., R. G. Shah, and G. G. Poirier.** 1996. Different cleavage pattern for poly(ADP-ribose) polymerase during necrosis and apoptosis in HL-60 cells. Biochem. Biophys. Res. Commun. **229:**838–844.
59. **Shi, Y., J. S. Lee, and K. M. Galvin.** 1997. Everything you have ever wanted to know about Yin Yang 1. Biochim. Biophys. Acta **1332:**F49–F66.
60. **Shi, Y., E. Seto, L. S. Chang, and T. Shenk.** 1991. Transcriptional repression by YY1, a human GLI-Kruppel-related protein, and relief of repression by adenovirus E1A protein. Cell **67:**377–388.
61. **Shikama, N., W. Lutz, R. Kretzschmar, N. Sauter, J. F. Roth, S. Marino, J. Wittwer, A. Scheidweiler, and R. Eckner.** 2003. Essential function of p300 acetyltransferase activity in heart, lung and small intestine formation. EMBO J. **22:**5175–5185.
62. **Shrivastava, A., S. Saleque, G. V. Kalpana, S. Artandi, S. P. Goff, and K. Calame.** 1993. Inhibition of transcriptional regulator Yin-Yang-1 by association with c-Myc. Science **262:**1889–1892.
63. **Sphyris, N., and D. J. Harrison.** 2005. p53 deficiency exacerbates pleiotropic mitotic defects, changes in nuclearity and polyploidy in transdifferentiating pancreatic acinar cells. Oncogene **24:**2184–2194.
64. **Srinivasan, L., X. Pan, and M. L. Atchison.** 2005. Transient requirements of YY1 expression for PcG transcriptional repression and phenotypic rescue. J. Cell. Biochem. **96:**689–699.
65. **Sui, G., E. B. Affar, Y. Shi, C. Brignone, N. R. Wall, P. Yin, M. Donohoe, M. P. Luke, D. Calvo, and S. R. Grossman.** 2004. Yin Yang 1 is a negative regulator of p53. Cell **117:**859–872.
66. **Sui, G., C. Soohoo, E. B. Affar, F. Gay, Y. Shi, and W. C. Forrester.** 2002. A DNA vector-based RNAi technology to suppress gene expression in mammalian cells. Proc. Natl. Acad. Sci. USA **99:**5515–5520.
67. **Takahashi, K., and K. Nakayama.** 2000. Mice lacking a CDK inhibitor, p57Kip2, exhibit skeletal abnormalities and growth retardation. J. Biochem. (Tokyo) **127:**73–83.
68. **Thomas, M. J., and E. Seto.** 1999. Unlocking the mechanisms of transcription factor YY1: are chromatin modifying enzymes the key? Gene **236:**197–208.
69. **Tsuchihara, K., V. Lapin, C. Bakal, H. Okada, L. Brown, M. Hirota-Tsuchihara, K. Zaugg, A. Ho, A. Itie-Youten, M. Harris-Brandts, R. Rottapel, C. D. Richardson, S. Benchimol, and T. W. Mak.** 2005. Ckap2 regulates aneuploidy, cell cycling, and cell death in a p53-dependent manner. Cancer Res. **65:**6685–6691.
70. **Uetake, Y., and G. Sluder.** 2004. Cell cycle progression after cleavage failure: mammalian somatic cells do not possess a "tetraploidy checkpoint." J. Cell. Biol. **165:**609–615.
71. **Vega, M. I., S. Huerta-Yepez, A. R. Jazirehi, H. Garban, and B. Bonavida.** 2005. Rituximab (chimeric anti-CD20) sensitizes B-NHL cell lines to Fas-induced apoptosis. Oncogene **24:**8114–8127.
72. **Vega, M. I., A. R. Jazirehi, S. Huerta-Yepez, and B. Bonavida.** 2005. Rituximab-induced inhibition of YY1 and Bcl-xL expression in Ramos non-Hodgkin's lymphoma cell line via inhibition of NF-kappaB activity: role of YY1 and Bcl-xL in Fas resistance and chemoresistance, respectively. J. Immunol. Methods **175:**2174–2183.
73. **Vergnes, L., M. Peterfy, M. O. Bergo, S. G. Young, and K. Reue.** 2004. Lamin B1 is required for mouse development and nuclear integrity. Proc. Natl. Acad. Sci. USA **101:**10428–10433.
74. **Wang, L., Q. Wu, P. Qiu, A. Mirza, M. McGuirk, P. Kirschmeier, J. R. Greene, Y. Wang, C. B. Pickett, and S. Liu.** 2001. Analyses of p53 target genes in the human genome by bioinformatic and microarray approaches. J. Biol. Chem. **276:**43604–43610.
75. **Wong, C., and T. Stearns.** 2005. Mammalian cells lack checkpoints for tetraploidy, aberrant centrosome number, and cytokinesis failure. BMC Cell. Biol. **6:**6.
76. **Wu, F., and A. S. Lee.** 2001. YY1 as a regulator of replication-dependent hamster histone H3.2 promoter and an interactive partner of AP-2. J. Biol. Chem. **276:**28–34.
77. **Yakovleva, T., L. Kolesnikova, V. Vukojevic, I. Gileva, K. Tan-No, M. Austen, B. Luscher, T. J. Ekstrom, L. Terenius, and G. Bakalkin.** 2004. YY1 binding to a subset of p53 DNA-target sites regulates p53-dependent transcription. Biochem. Biophys. Res. Commun. **318:**615–624.
78. **Yang, D., A. Welm, and J. M. Bishop.** 2004. Cell division and cell survival in the absence of survivin. Proc. Natl. Acad. Sci. USA **101:**15100–15105.
79. **Yao, T. P., S. P. Oh, M. Fuchs, N. D. Zhou, L. E. Ch'ng, D. Newsome, R. T. Bronson, E. Li, D. M. Livingston, and R. Eckner.** 1998. Gene dosage-dependent embryonic development and proliferation defects in mice lacking the transcriptional integrator p300. Cell **93:**361–372.
80. **Yao, Y. L., W. M. Yang, and E. Seto.** 2001. Regulation of transcription factor YY1 by acetylation and deacetylation. Mol. Cell. Biol. **21:**5979–5991.
81. **Zhang, P., N. J. Liegeois, C. Wong, M. Finegold, H. Hou, J. C. Thompson, A. Silverman, J. W. Harper, R. A. DePinho, and S. J. Elledge.** 1997. Altered cell differentiation and proliferation in mice lacking p57KIP2 indicates a role in Beckwith-Wiedemann syndrome. Nature **387:**151–158.
82. **Zhou, Q., and D. A. Engel.** 1995. Adenovirus E1A243 disrupts the ATF/CREB-YY1 complex at the mouse c-*fos* promoter. J. Virol. **69:**7402–7409.
83. **Zhou, Q., R. W. Gedrich, and D. A. Engel.** 1995. Transcriptional repression of the c-*fos* gene by YY1 is mediated by a direct interaction with ATF/CREB. J. Virol. **69:**4323–4330.